THE EFFECTS OF STATIC AEROELASTICITY ON
THE PERFORMANCE
OF
TWO-DIMENSIONAL CONVERGING DIVERGING NOZZLES

A THESIS SUBMITTED TO
THE GRADUATE SCHOOL OF NATURAL AND APPLIED SCIENCES
OF
MIDDLE EAST TECHNICAL UNIVERSITY

BY

ÜMRAN DÜZEL

IN PARTIAL FULFILLMENT OF THE REQUIREMENTS
FOR
THE DEGREE OF MASTER OF SCIENCE
IN
AEROSPACE ENGINEERING

FEBRUARY 2014

Approval of the thesis:

**THE EFFECTS OF STATIC AEROELASTICITY ON
THE PERFORMANCE OF
TWO-DIMENSİONAL CONVERGING DIVERGING NOZZLES**

submitted by **ÜMRAN DÜZEL** in partial fulfillment of the requirements for the degree of **Master of Science in Aerospace Engineering Department, Middle East Technical University** by,

Prof. Dr. Canan Özgen
Dean, Graduate School of **Natural and Applied Sciences** _____

Prof. Dr. Ozan Tekinalp
Head of Department, **Aerospace Engineering** _____

Assoc. Prof. Dr. Sinan Eyi
Supervisor, **Aerospace Engineering Dept., METU** _____

Examining Committee Members

Prof. Dr. Sinan Akmandor
Aerospace Engineering Dept., METU _____

Assoc. Prof. Dr. SİNAN EYİ
Aerospace Engineering Dept., METU _____

Prof. Dr. Altan Kayran
Aerospace Engineering Dept., METU _____

Assoc. Prof. Dr. D.Funda Kurtuluş
Aerospace Engineering Dept., METU _____

Y.Müh Korhan Alpan
ROKETSAN, INC _____

Date: **06.02.2014**

I hereby declare that all information in this document has been obtained and presented in accordance with academic rules and ethical conduct. I also declare that, as required by these rules and conduct, I have fully cited and referenced all material and results that are not original to this work.

Name, Last name: ÜMRAN DÜZEL

Signature:

ABSTRACT

THE EFFECTS OF STATIC AEROELASTICITY ON
THE PERFORMANCE OF
TWO-DIMENSİONAL CONVERGING DIVERGING NOZZLES

DÜZEL, Ümran

M.S., Department of Aerospace Engineering

Supervisor: Assoc. Prof. Dr. Sinan EYİ

February 2014, 60 Pages

This thesis analyzes the effects of static aeroelasticity on the performance of two dimensional converging diverging nozzles. A Flow analysis is conducted on five different configurations of two dimensional converging-diverging nozzles. Computational study is validated with experimental data. Two of the configurations, which have the same throat area, throat radius, and convergence angle and total nozzle length, are selected as the baseline geometries. By modifying throat radius and keeping all other geometric parameters to be the same, three more configurations are obtained so that throat contouring can be examined as well.

 Flow analyses are performed by using FLUENT flow solver software. By considering nozzle walls as flexible structure, a static aeroelastic model is implemented. Stiffness, coordinate system transformation, force vector matrices have been obtained for structural model. The flexible wall implementation uses two-dimensional linear beam model. The results of flexible and rigid walls are compared for different nozzle thicknesses. Axisymmetric cases are added to the model to present the differences.

Keywords: Static Aeroelasticity, Converging Diverging Nozzles, FLUENT, Stiffness Matrix, Linear Beam Theory

ÖZ

STATİK AEROELASTİSİTENİN İKİ BOYUTLU YAKINSAK IRAKSAK LÜLE PERFORMANSINA ETKİSİ

DÜZEL, Ümran

Yüksek Lisans, Havacılık ve Uzay Mühendisliği Bölümü

Tez Yöneticisi: Doç. Dr. Sinan EYİ

Şubat 2014, 60 sayfa

Bu tez çalışmasında statik aeroelastisitenin iki boyutlu yakınsak ıraksak lüle performansına olan etkisi ele alınmıştır. Çalışmada; 5 farklı lüle konfigürasyonu incelenmiştir. Analiz sonuçları deneysel verilerle karşılaştıtılarak doğrulama yapılmıştır. Lüle konfigurasyonlarından lüle boğaz yarıçapı, lüle boğaz alanı, yakınsama açısı ve lüle boyu aynı olan iki konfigurasyon baz geometri seçilmiştir.Diğer üç konfigurasyon baz geometrilerin tüm parametreleri aynı kalacak şekilde boğaz yarıçağı değiştirilerek oluşturulmuştur boylece boğaz yarıçaplarının etkiside incelenebildi.

Akış analizi FLUENT hazır ticari kod kullanarak yapılmıştır. Lüle duvarının esnek yapı olduğu düşünülerek aeroelastik modelleme yapılmış ve uygulanmıştır. Esnek yapı modeli iki boyutlu lineer kiriş olarak modellenmiştir. Esnek lüle duvarı ile esnemez, rigid, lüle duvarı sonuçları farklı lüle duvar kalınlıklarıyla karşılaştırılmıştır.

Anahtar kelime; Statik Aeroelastisite, yakınsak-ıraksak lüle, FLUENT, direngenlik matrisi, lineer kiriş teorisi

To My Family

ACKNOWLEDGMENTS

TABLE OF CONTENTS

LIST OF TABLES

TABLES

LIST OF FIGURES

FIGURES

LIST OF SYMBOLS

$C\text{-}D$	=	convergent-divergent
A_1	=	low divergence angle nozzle configuration
A_2	=	low divergence angle nozzle configuration
B_1	=	high divergence angle nozzle configuration
B_2	=	high divergence angle nozzle configuration
B_3	=	high divergence angle nozzle configuration
A_e	=	nozzle exit area
A_t	=	nozzle throat area
A_e / A_t	=	nozzle expansion ratio
l	=	nozzle length
M_d	=	design Mach number
p_t	=	total pressure
p_∞	=	ambient pressure
p_t / p_∞	=	pressure ratio
r_c	=	nozzle circular arc throat radius
θ	=	convergence angle
ε	=	divergence angle
h_e	=	half height at nozzle exit
h_i	=	half height at nozzle inlet
h_t	=	half height at nozzle throat
d_n^l	=	displacement in local coordinate
f_n^l	=	Force vector in local coordinate
k_e	=	element stiffness matrix

v_{ix}	=	deflection component at node i
v_{iy}	=	deflection component at node i
v_{iz}	=	deflection component at node i
E	=	Young Modulus
L	=	length of beam
τ_w	=	wall shear stress
P	=	flow pressure

LIST OF ABBREVIATIONS

CFD	:	Computational Fluid Dynamics
FEM	:	Finite Element Methods
CSD	:	Computational Structural Dynamics
DOF	:	Degree of Freedom

CHAPTER 1

INTRODUCTION

1.1.INTRODUCTION

THe increasing demand for developing jet engines brings new challenges to develop highly efficient nozzles. Since most of the thrust is produced in nozzle, the accurate calculation of nozzle performance is important. Most of the nozzles operate at high temperature and in chemically reacting flows. There are also strong interactions between these flows and solid surfaces. These interactions take place between structural, aerodynamic and inertial forces which can cause several phenomena. One of the most important phenomena to deal with is static aeroelastic phenomena that results in quite considerable elastic deformation. Simply the flow interacts with structure causes local and global change in the existing geometry hence the result will affect the subsequent flow of the fluid. Detailed work of fluid-structure/solid-interaction (FSI) multi-physics is mostly required to analyze these interactions and observe the consequences. The performance of nozzle is affected by these consequences and an accurate aeroelastic modeling is needed for that kind of nozzles.

The scope of this study is to analyze, observe the static aeroelastic effects in nozzles and how the results affect the performance. For the case of aeroelastic analysis, the nozzle wall is considered as flexible two dimensional

linear beam elements. A finite element analysis by direct stiffness method is used to calculate the displacement under static load. Five different configurations of two-dimensional (non-axisymmetric) converging diverging nozzles are examined by flow analysis and one of the nozzles cases is implemented to be solved structurally. The solution procedure is based on loosely-coupled method. The first part of this work mainly focuses on the computational fluid dynamics analysis of nozzles and the validation with experimental data. One of the selected nozzle configurations is created and a structural type grid is constructed in geometry domain. A commercial software (FLUENT) is used for flow analysis. In all cases, the ratio of inlet total pressure to exit static pressure, which is called nozzle pressure ratio, are set to be 7.97. The same pressure ratio is selected for all configurations to be consistent. Initially, the nozzle wall is assumed to be rigid, and the results are validated with experimental data of Langley 16 foot transonic tunnel. In the second part, the nozzle wall is considered as flexible structure, and an aeroelastic analysis is performed. In these configurations, there is no experimental data for flexible wall. The effects of aeroelasticity on nozzle performance are investigated by comparing the flexible wall results with rigid wall results.

1.2. MOTIVATION

Computational fluid dynamics an acronym that refers to CFD is the largest user of high-performance computing in engineering field. CFD now became an indispensable analysis/design/optimization tool in the very large range of industrial applications. Flow problems are often so complex that a high level of ingenuity is required and essential. Thus, besides the development work in CFD, innovative CFD applications are also encouraged.

Finite element method, FEM, is the complementary branch with computational fluid dynamics for high performance computing in engineering field. In the last few decades advances and progresses in the field of computer aided engineering have been quite extensive and have led to considerable benefits mostly to aerospace industries. In the aerospace field, use of advanced finite element tools has allowed the introduction of innovative and efficient products. High performance computing and advanced finite element tools became vital for research and development activities in many universities and industries. Development of hardware has made finite element analysis very efficient and complexibility of problems became trivial.

Application of computational fluid and finite element analysis became an essential part of design and optimization of aerospace engineering as well for other engineering fields. The increasing use of high performance components such as jet engines, nozzles, wing configurations...etc. requires a wide range of designer review. One of the design requirements is to work with CFD and FEM iteratively. Several computational methods for structure fluid interactions have been developed to different levels of problem complexibility. Investigation of flow-structure, structure-flow interactions and their effects on each other is the primary goal in design phases. Performance is highly depended on the interactions of fluid and solid. Determination of the magnitude of the dependency will help to improve the efficiency.

1.3. LITERATURE SURVEY

Aeroelasticity effect takes place everywhere that the fluid and structure cannot be considered independently to predict the response of the fluid, the structure, or both. Several work conducted on aeroelastic effect throughout decades can be found in the literature. Aeroelasticity has been conducted on the field of aerospace; spacecraft, aircrafts, rotorcrafts, compressors, combustors, turbines, civil structures; bridges, towers, buildings, dams, transportations; ships, trains, automobiles, medicine; veins, arteries, heart, marine; off-shore platforms, docks, piers, and computer technology high velocity flexible storage devices[1]. The flow and structure interactions became a vital part of development since the importance of it has been understood after failures and disasters happened in the history of mankind. Below some significant aeroelasticity problems in rocket technology, especially in nozzle area, will be presented before flow structure interactions were considered as a critic design parameters.

Improvement in missile design has been growing with requirements of more flexibility, higher speeds, and high maneuverability. To this, interdisciplinary research of fluid, structural analysis has been conducted for missiles, rockets and for their components.

A work done by Mason et al., 1986 [2] is to investigate and develop a tool for analytically treating the aeroelastic stability of rocket nozzle. To solve the problems they obtained the equation of motion, stiffness and aerodynamic matrix relations for rocket nozzle exit cones which was considered to be conical shells.

A general steady computational fluid dynamics code is modified to include aeroelastic effects by Karpel et al., 1998 [3] Static aeroelastic problems of maneuvering flight vehicles with non-linear aerodynamics, linear structure has been demonstrated by presenting a solution scheme. Figure 1 gives the results of deformed body and rigid body lift distribution. There occurs a slight difference in forces generated by the body.

4
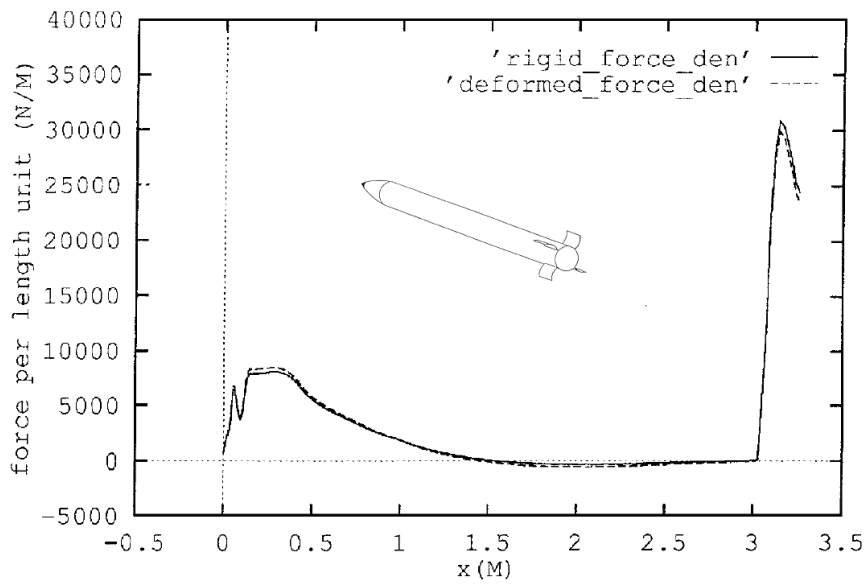
Figure 1 Lift Distribution of Deformed and Rigid Body [3].

An investigation is made to determine and observe the effect of body flexibility on aerodynamic coefficients by Harkins et al., 1990 [4]. The effects of body flexibility were estimated and the results were compared with experimental and rigid body data. Figure 2 indicates the results of the effects of body elasticity. According to Harkins, T. K., Courter, R. W. bending flexibility does not appreciably alter the values of aerodynamic coefficients but still it is a concern for further investigation.
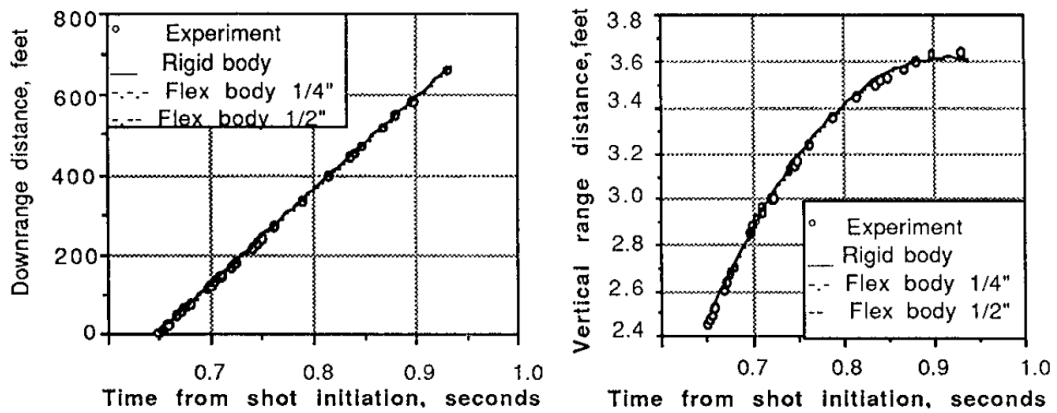
Figure 2 The Trajectories Change Due to Coefficients Deviation [4].

5

The influence, importance and development of investigation of aeroelasticity and its effects on the performance is briefly illustrated above. The range its influence and effects widely much. The understanding of aeroelastic response is critical in every part of design. The historical investigation is briefly presented above.

The deviation of nozzle performance due to aeroelastic influences was investigated by many scientists and researchers. Some conducted study clearly shows the importance of aeroelasticity on nozzle performance. Felker, F. Fort [5] developed a method for static aeroelasticity problems and in this case he solved two dimensional nozzles in order to describe the effects. In his method the discretized fluid dynamic and structural equations is a single set of coupled, nonlinear equations. Newton's method was used to obtain the equilibrium solution. The equations used for flow solution are two dimensional Navier-Stokes equations. A finite element method was used for structural solution. The direct solution was implemented to the method. The calculations were conducted by assuming the nozzle walls were flexible and the results compared with rigid walls. As a result he concluded that the change in nozzle geometry had significant effect on the flow inside the nozzle. Thus the change resulted in performance alter. The flexible wall geometry change due to structure flow interactions is presented in Figure 3 for different wall thicknesses.
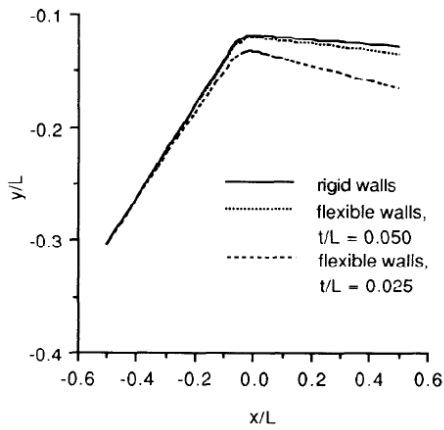
Figure 3 Rigid and Flexible Nozzle Wall Changes [5]

The study also shows that wall flexibility changed the nozzle expansion ratio with a favorable manner. This is clearly presented in Figure 4 which shows Mach number increase.
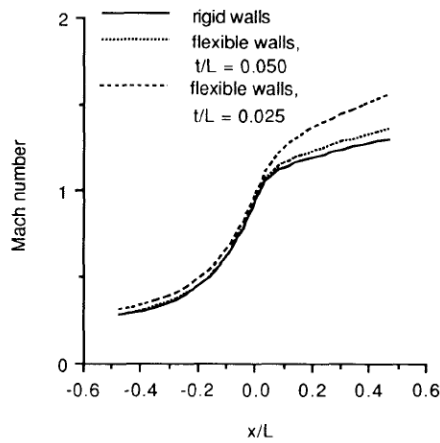
Figure 4 Mach Number with Rigid and Flexible Nozzle Walls [5]

The work conducted above by Felker, F. Fort can be supported much later with a study carried out by Zhao et al., 2012 [6]. The aeroelastic response of rocket nozzles subjected to combined axial thrust and side loads is calculated by using loose coupling method between flow solver and structural-dynamics solver.

Zhao divided the problem into three components which are;

- Modeling fluid dynamic part
- Modeling structural dynamic part
- Coupling of the fluid dynamic and structural dynamic part

The scope of the study is to investigate the behavior of the internal flow, the behavior of the nozzle wall, and the interactions between the fluid-dynamic and structural-dynamic phenomena. 1/16-scale nozzle of a J-2S rocket engine[6] with an area ratio of 39.6, a length of 2228.088 mm, and a throat radius of 154.94 mm was used as the case study. Rigid walls and flexible walls were analyzed and compared to illustrate the flow structure interaction in rocket nozzle.
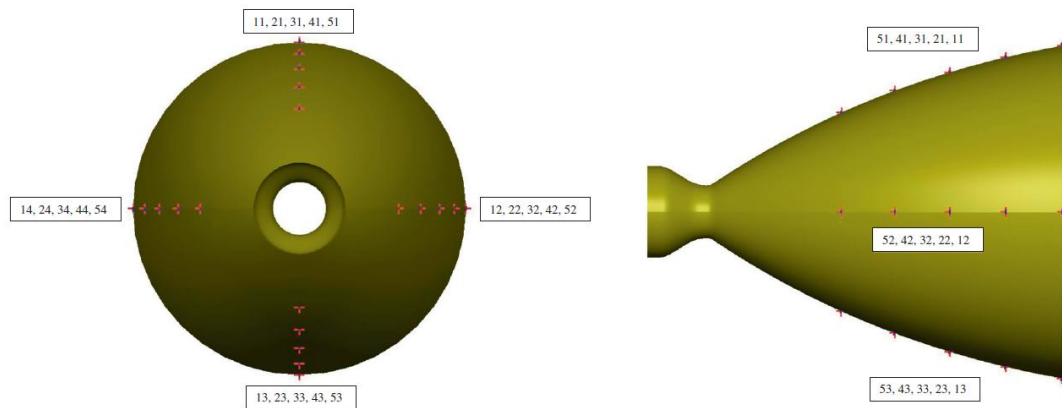
Figure 5 The Distribution of Points Monitor Around The Nozzle Wall [6].

Figure 5 shows the monitoring nodal points that were used for evaluation of the   wall pressure and the wall displacements of the nozzle. The results presented as the ratio of the static wall pressure, P_w, to the static chamber pressure, P_c for both rigid and flexible wall, see Figure 6 . Figure 7 presents wall displacement at given node points, see Figure 5.
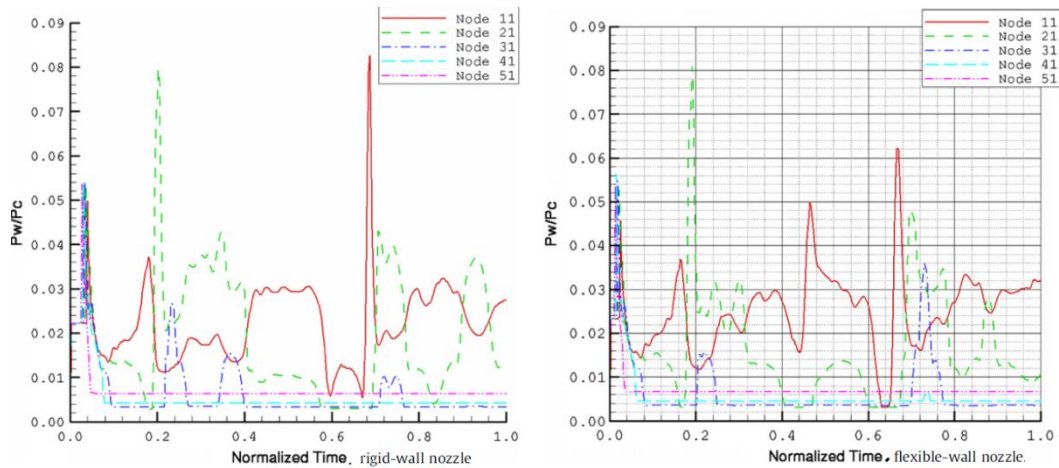
Figure 6 Wall Pressure Variations with Time for Nozzle J-2S [6].
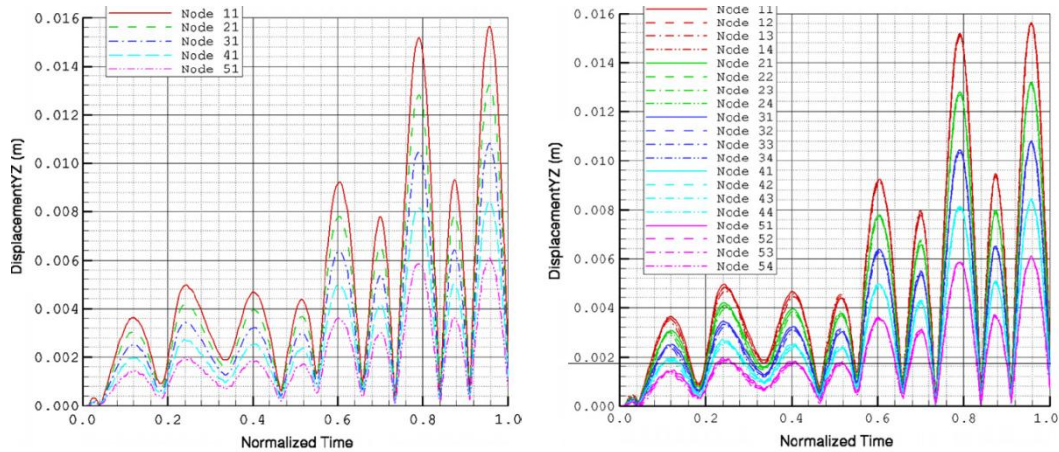
Figure 7 Wall Displacements with Time for Flexible Nozzle Wall [6].

From the results it can be seen that the wall pressure results are almost similar for the two cases. However, the highest peak of the wall pressure with the rigid-wall case is smaller than the corresponding value for the flexible-wall. Moreover, for the flexible-wall case, the peak occurs at different node. Oscillation of the flexible nozzle wall can be interpreted from the results. The vibration can be seen clearly. A two way loose coupling methodology between CFD and CSD were implemented to study fluid–structural interactions in rocket nozzle. Results suggest that aeroelastic effects should not be ignored in the design or analysis phase of nozzle developments.

9

A study conducted by Garelli et al., 2009 [7] mainly focuses on aeroelastic processes evolved on the phase of starting a rocket engine. The study presents the behavior of the structure inside the engine nozzle. Euler equations and linear elastic solid adaptation were implemented for fluid and structure. Gaus-Seidel algorithm was evaluated over flow and structure. Brief results of the study and aeroelastic behaviors of the rocket nozzle are illustrated in Figure 8, Figure 9 and Figure 10.
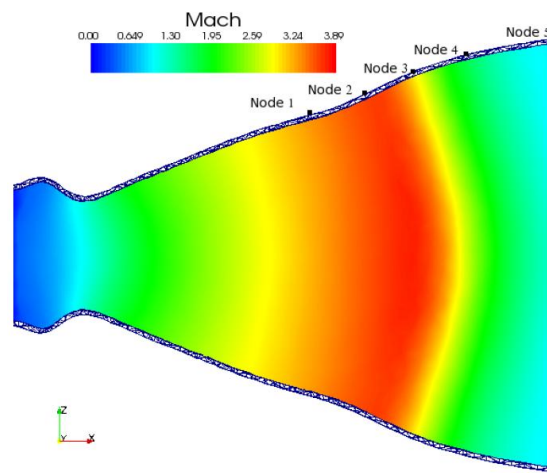
Figure 8 Nozzle Structure Deformation [7].
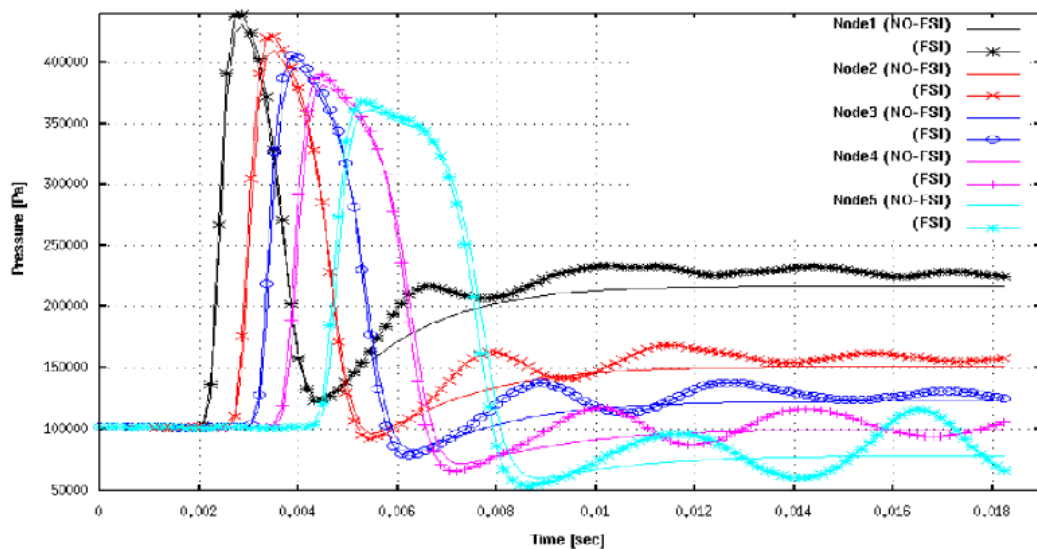
Figure 9 Wall Pressure Values with FSI and No-FSI [7].

10

The aeroelastic behavior and effects were analyzed by coupling fluid-structure codes. The study pointed out that considering the wall displacement to compute the pressure changes inside the nozzle is a key point for performance optimization.
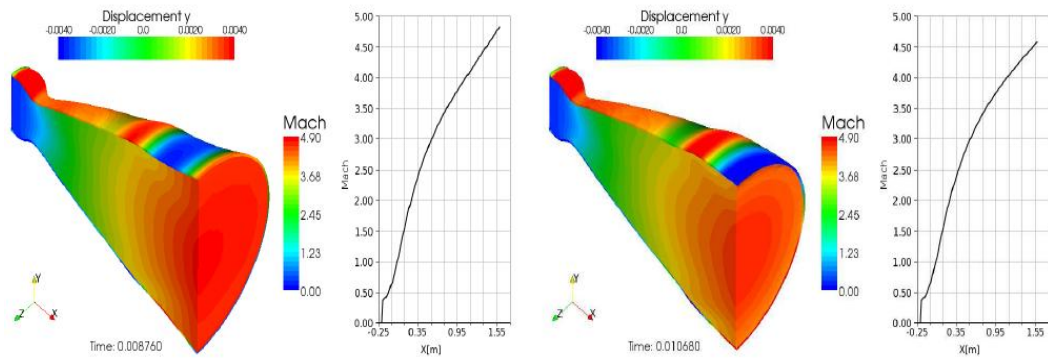
Figure 10 Rocket Ignition Processes [7].

1.4.OUTLINE OF THE THESIS

This thesis is organized in five chapters. Brief explanation of the chapters is as follows;

Chapter 1 includes the introduction of the study. The scope of the study and the procedure of the work are stated. Motivation of the thesis is presented in the coming pages. Review of prior researches, analysis and investigations are stated.

Chapter 2 includes nozzle design and experimental set up. The nozzle configurations that will be examined are stated in this section. Also experimental results of the nozzles will be given in this chapter. Grid generation and determination of its size is explained. Solutions is obtained by flow solver FLUENT are stated in this part. Validation of the flow analysis is presented by presenting experimental data.

Chapter 3 focuses on structural study. Stiffness matrix construction, coordinate transformation and the aerodynamic load formulations are stated in this chapter. Matrix properties are also stated in this chapter.

Chapter 4 gives the performance changes of the flexible wall nozzles as a result of the study. Performance parameters have been compared for rigid and flexible walls.

Chapter 5 contains the conclusion of the work conducted. It also gives a summary for the study completed. Recommendations are presented for the directions of future research.

CHAPTER 2

FLOW ANALYSIS

2.1.NOZZLE CONFIGURATIONS

In this investigation, five 2-D (non-axisymmetric) and C-D nozzles geometries are analyzed and the computational solutions are compared with experimental data in order to validate the commercial fluid solver package. Two of the nozzles (A_1 and B_1) are the baseline geometries [8]. The other geometries (A_2, B_2 and B_3) are evaluated by modifying design parameters of the baseline geometries. Configurations A_1 and B_1 have the same throat area, throat radius, total nozzle length and convergence angle. Modification has been done by increasing throat radius only. During the modifications all other parameters are kept as constant except the converging diverging angles. The radius of baseline configurations is 0.68cm. In configurations A_2 and B_2, the radius is increased from 0.68 cm to 2.74 cm. Radius in configurations A_2 and B_2 are 2.74cm. In the last configuration, B_3, the radius is 2.74cm, and divergence angle, ε is kept constant. The design parameters for nozzle geometries are sketched in Figure 11. Summary of the geometric parameters of the configurations are given in Table 1 . All length units are centimeter.
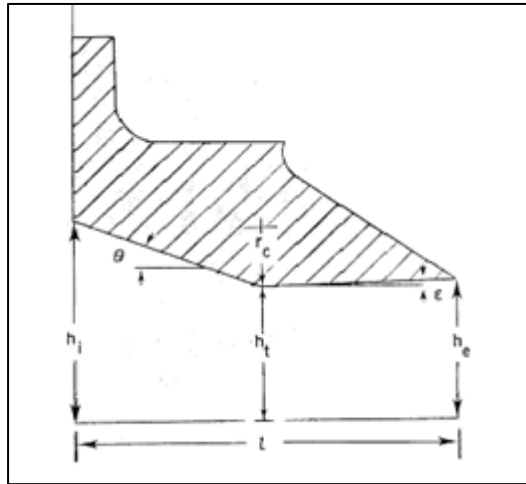
Figure 11 2D Sketch of Nozzles

Table 1 Configuration Parameters

Parameters	A$_1$	A$_2$	B$_1$	B$_2$	B$_3$
h_i	3.52	3.52	3.52	3.52	3.52
h_e	1.49	1.49	2.46	2.46	2.46
h_t	1.37	1.37	1.37	1.37	1.37
r_c	0.68	2.74	0.68	2.74	2.74
A_e / A_t	1.09	1.09	1.80	1.80	1.80
l, cm	11.56	11.56	11.56	11.56	12.25
M_d	1.35	1.35	2.08	2.08	2.08
p_t / p_∞	2.97	8.81	8.81	8.81	8.81
$\theta, ^\circ \deg$	20.84	22.33	20.84	22.33	20.42
$\varepsilon, ^\circ \deg$	1.21	1.21	10.85	11.24	10.85

2.2. EXPERIMENTAL SETUP

The nozzle performances were tested by the static test facility of Langley 16 foot transonic tunnel. The test setup is located in a room with high ceiling and a wide, large open doorway [9] .An external high-pressure air system provides a continuous flow of clean and dry air which is kept at a controlled temperature of 300 K and pressurized up to 1013 kPa. Figure 12 shows the experimental setup for nozzle configuration A$_1$, A$_2$ and B$_1$. Result of the experiment can be obtained from NASA Technical Report [8].

14
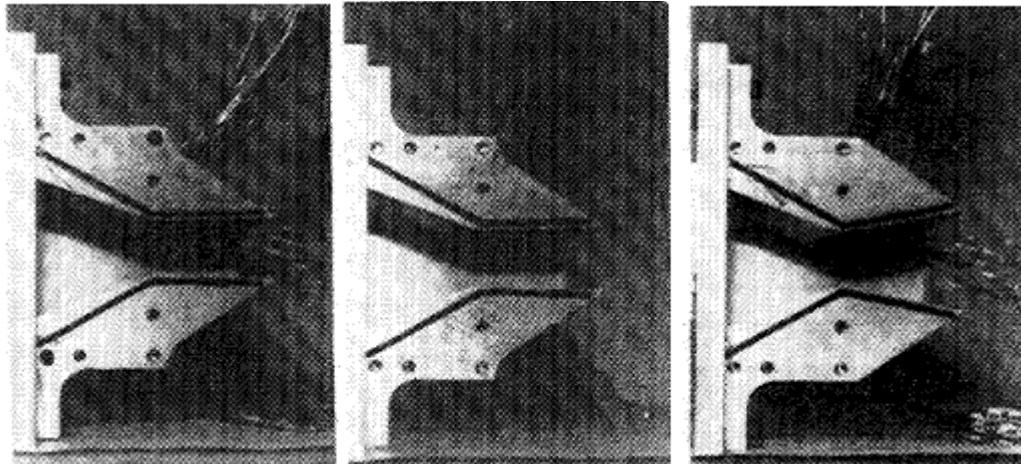
Figure 12 Test Setup of Nozzles A_1, A_2 and B_1[8].

2.3. GRID GENERATION

As a mesh generator tool, GAMBIT is used to create the grid. Structured grid has been created for nozzle configurations. This type of mesh provides sufficient accuracy as well as increased computational performance. Before selecting the right, good mesh; a study conducted on grid size and its effect on solutions. A good determined mesh will help the flow solver converge to most accurate solution at the mean time however the computer resources, time will expand. In this case different mesh sizes vary from very coarse to fine has been selected. Figure 13 shows results of different size meshes which are 48x20, 72x30, 100x40, 160x80 and 240x100. From the Figure 13 and Figure 14 can be interpreted that as the mesh gets finer and finer more accurate solution can be obtained until a limit. After a while even if we increased the grid density the results will not be affected and it will converge to a steady solution. Increasing the mesh density will increase the iterations and convergence time. It should be known that the practical matter of minimizing compute time should be achieved by using the minimum and optimum number of grid points. As a result obtained from different mesh sizes, we are able to set our grid and be satisfied to have 100 and 40 control volumes since grid dependency shows

15

almost no change in results after 100x40 grid points. This also will allow us save time even if we use we finest mesh to obtain the same accuracy.

Skin friction coefficient has been calculated for different mesh sizes. The results of skin friction coefficient also indicate that it converges to a steady solution. From the coarse to fine grid it oscillates until it reaches a steady value at the finest grid. Figure 15 presents how the skin friction coefficient varies with grid size. Reaching the supersonic regime results in oscillation until the mesh is set to be finest.

The mesh used in the presented study is shown in Figure 16 . In the stream-wise and cross-streamwise directions there are 100 and 40 control volumes, respectively. Mesh skewness is kept below 0.52 so that the quality, accuracy and efficiency can be provided well. Since there will be large pressure and velocity differentials across the throat and close to the nozzle wall quite fine mesh is required in these regions.   Nozzle boundary conditions are illustrated in Figure 17.
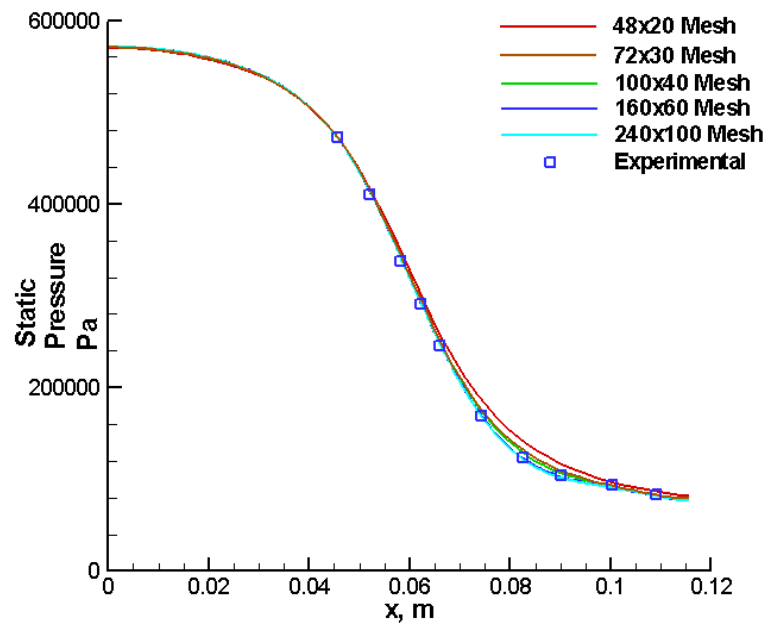
Figure 13 Grid Dependency Study, Nozzle Centerline Static Pressures
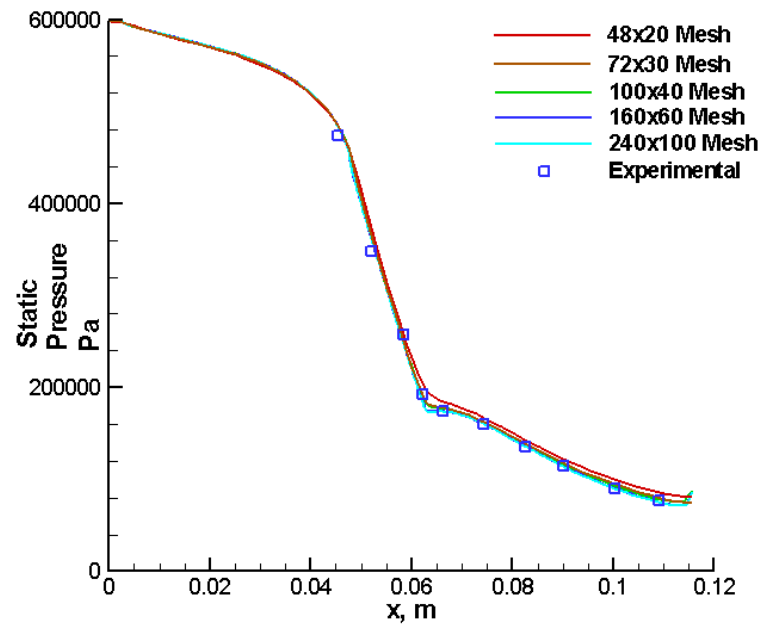
Figure 14 Grid Dependency Study, Nozzle Wall Static Pressures

17
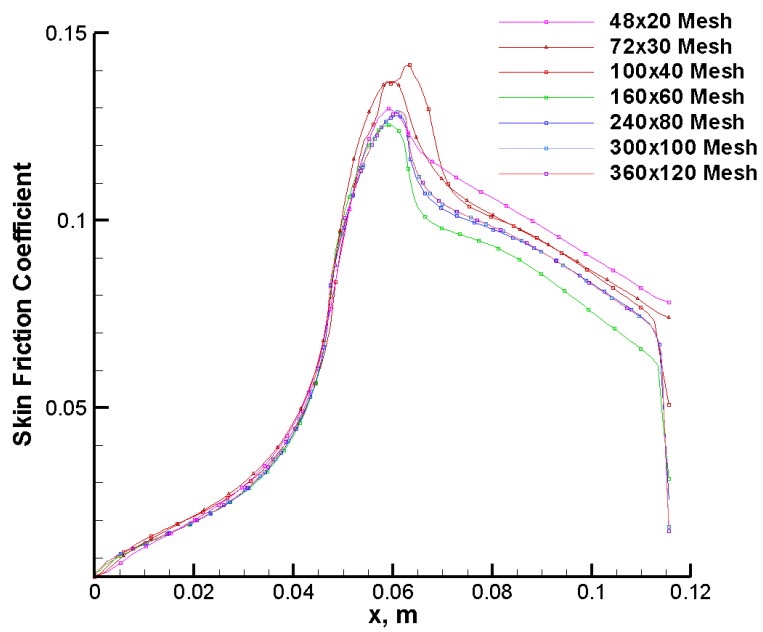
Figure 15 Skin Friction Coefficient Varying With Grid Size
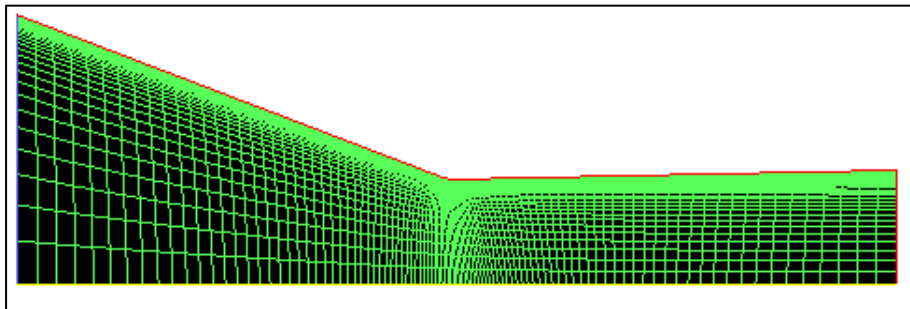
Figure 16 100x40 Generated Mesh
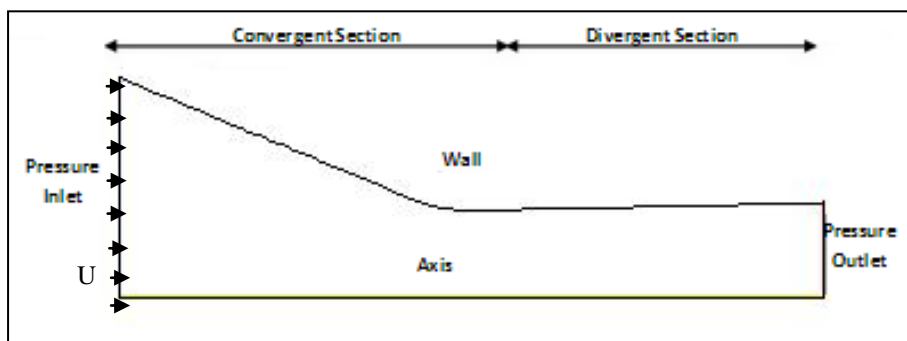
Figure 17 Nozzle Boundary Conditions

2.4. FLOW SOLUTION

Pressure based, 2-D, implicit solution method is utilized for all configurations. The solver uses an algorithm belongs to projection method [10]. In the projection method, the constraint of mass conservation (continuity) of the velocity field is achieved by solving a pressure (or pressure correction) equation [11]. The pressure equation is derived from the continuity and the momentum equations in such a way that the velocity field is corrected by the pressure to satisfy the continuity. Since the governing equations are nonlinear and coupled to one another, the solution process involves iterations wherein the entire set of governing equations is solved repeatedly until the solution converges to a steady state [11]. For the turbulence viscosity model three different types of models are implemented to examine the results at first. The models are K-epsilon ($k - \varepsilon$), K-omega ($k - \omega$) and Spalart-Allmaras. There modes are implemented and the results are presented in Figure 18.
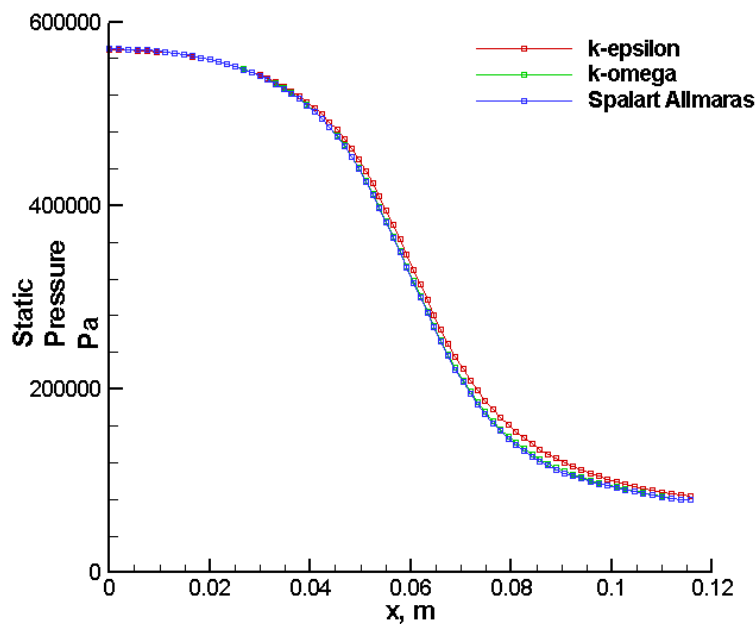
Figure 18 Turbulence Models Comparison at Nozzle Centerline
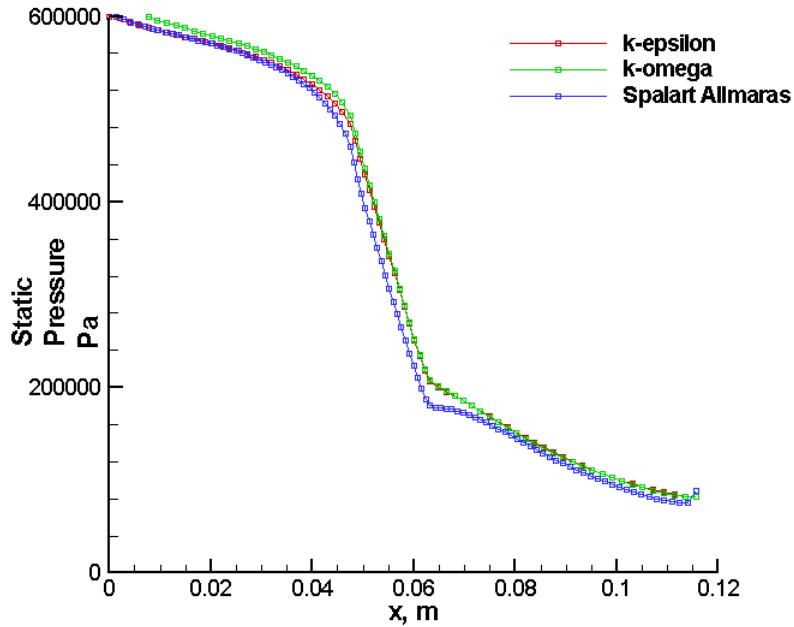
Figure 19 Turbulence Models Comparison at Nozzle Wall

Results of different turbulent models represent very good consistency with each other. However, the convergence took much longer time by K-epsilon ($k - \varepsilon$), K-omega ($k - \omega$) although they gave almost the exact values at nozzle centerline as Spalart-Allmaras did. Figure 19 gives better idea on turbulence models since the wall treatment will result in large turbulence weak.

In the study as a turbulence model Spalart-Allmaras equation is implemented since it will accurate results and time saving. Spalart-Allmaras model takes the distance to the closest wall as the definition for the length scale, which plays a major role in selecting the level of production and destruction of turbulent viscosity model. The boundary conditions specified at the inlet are the total temperature and the total pressure of air. At the centerline, symmetry and at the wall rigid wall boundary conditions are implemented. The nozzle pressure ratio is set to 7.95 for all configurations.

2..4.1. RIGID WALL FLOW SOLUTION

Figure 20, Figure 21 and Figure 23 presents the results obtained by flow solver for rigid wall nozzle B_1. Convergence history is stated in Figure 22.
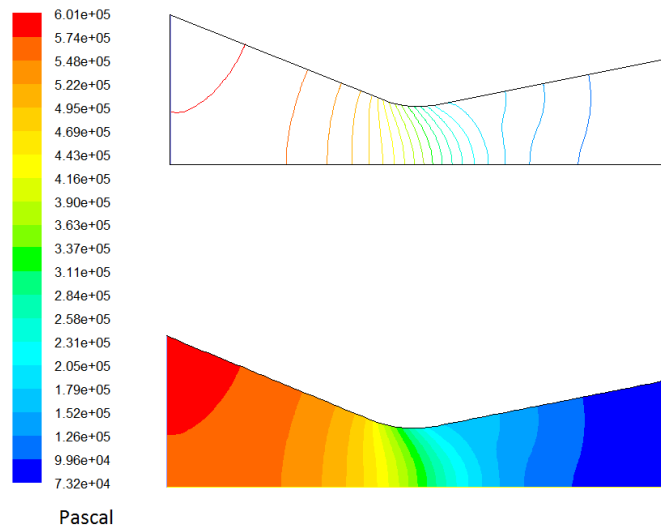
Figure 20 Contours of Static Pressure for Nozzle B_1
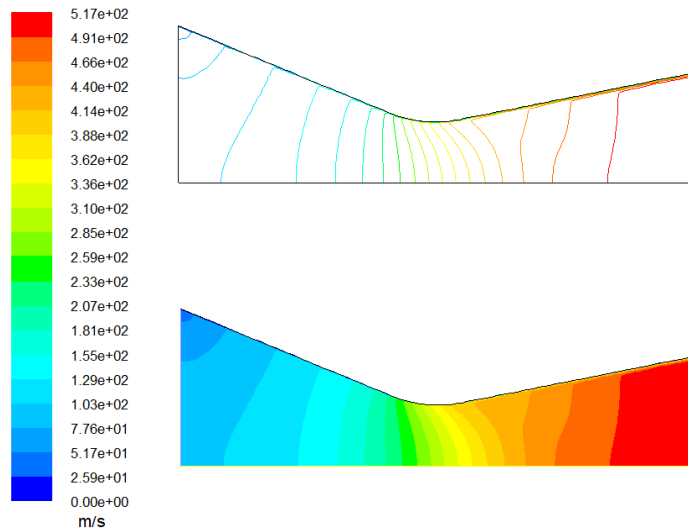
Figure 21 Contours of Velocity Magnitude for Nozzle B_1
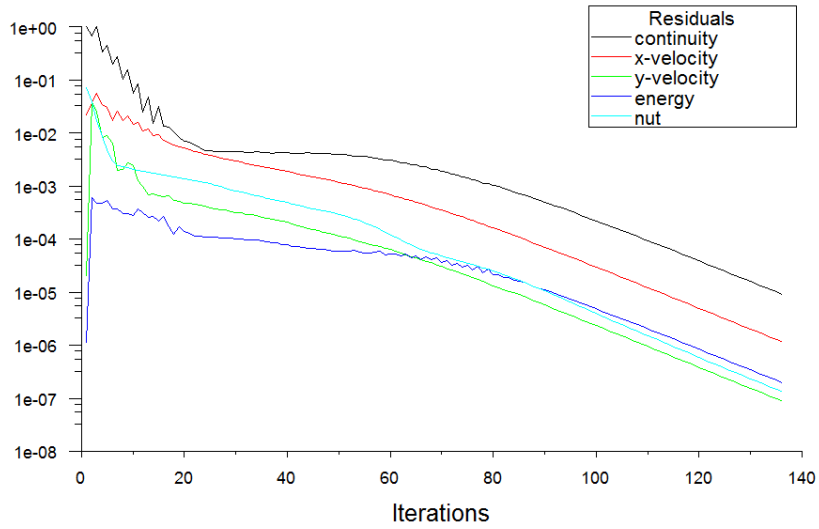
Figure 22 Convergence History

Solution converges after 140 iterations and the convergence criteria set to be 10^{-6}, see Figure 22. This is a well obtained convergence. The obtained pressure and velocity magnitude results are stated above and the best way to find how accurate we are is to compare the data with experimental results. All the result obtained and validated in this chapter is for rigid nozzle wall.
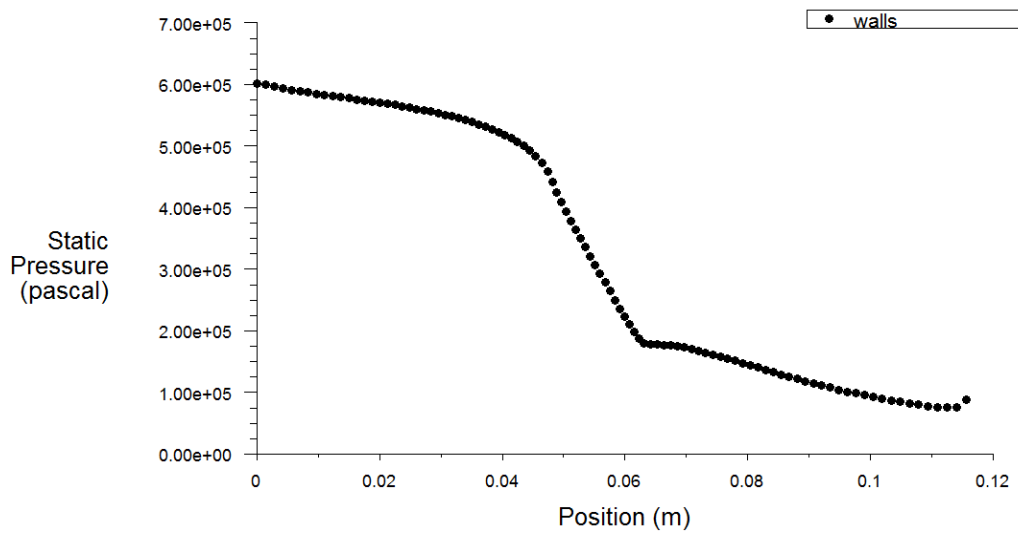
Figure 23 Static Pressure of the Nozzle Wall for B$_1$

22

2.5. VALIDATION OF THE RESULTS

Results obtained both form flow solver and experimental data is compared to see how accurate we are. The pressure ratios from the flow solver and experimental data are compared at the nozzle wall and at the centerline. Experimental data also can be seen from APPENDIX A, Figure A.1-A.10. Also in the APPENDIX A comparison of experimental data with two-dimensional inviscid theory has been stated [8].
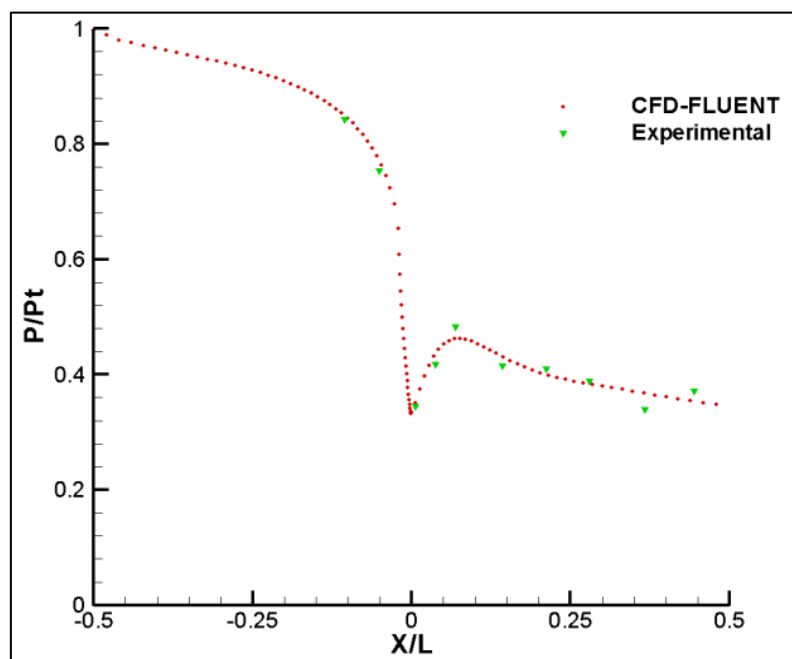
Figure 24 Results of Wall Pressure Ratio Nozzle A$_1$
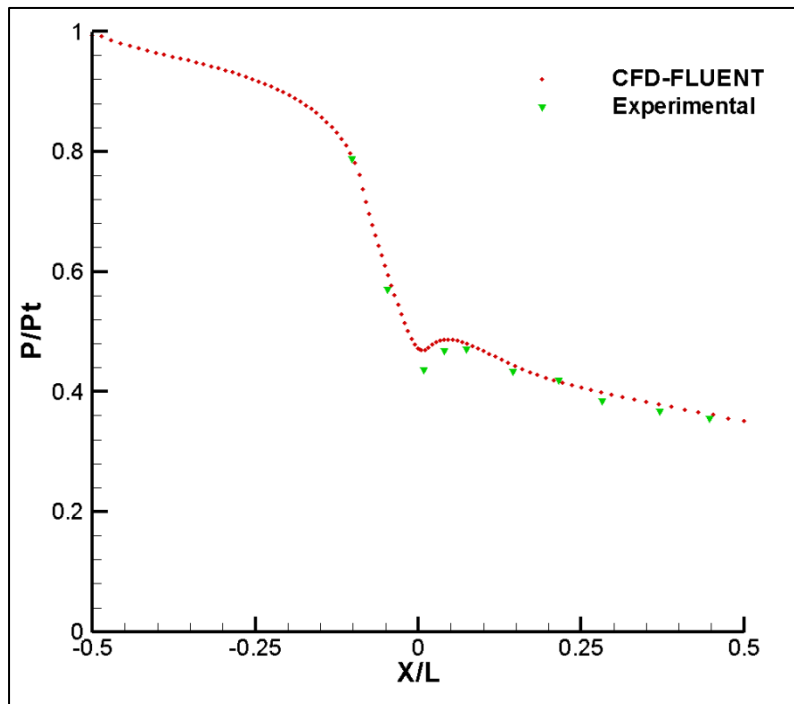
Figure 25 Results of Wall Pressure Ratio Nozzle A₂
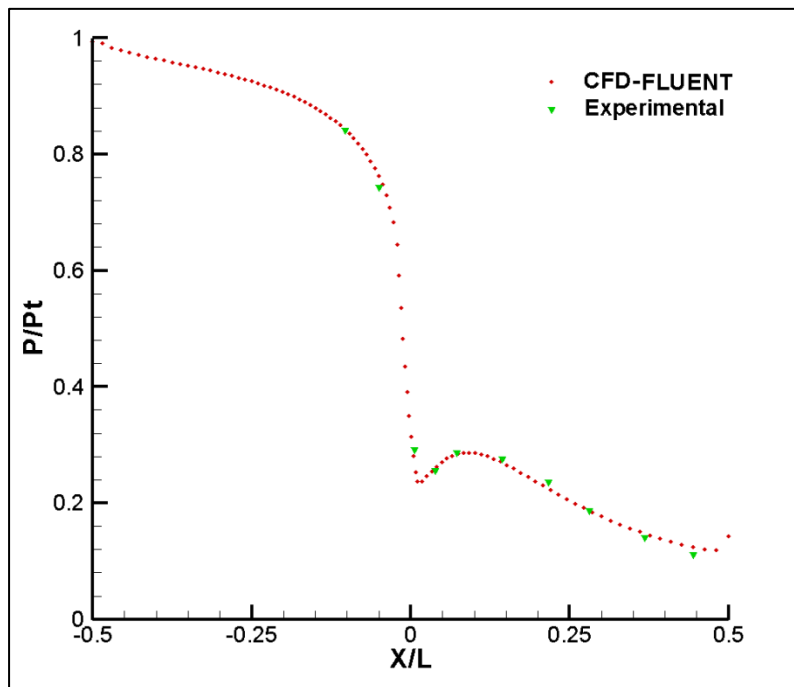
Figure 26 Results of Wall Pressure Ratio Nozzle B₁
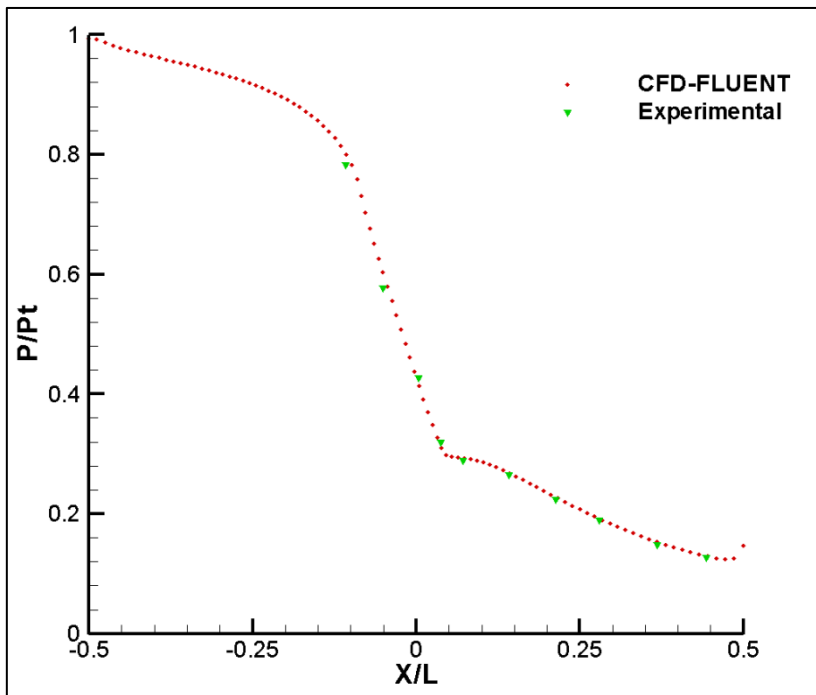
Figure 27 Results of Wall Pressure Ratio Nozzle B$_2$
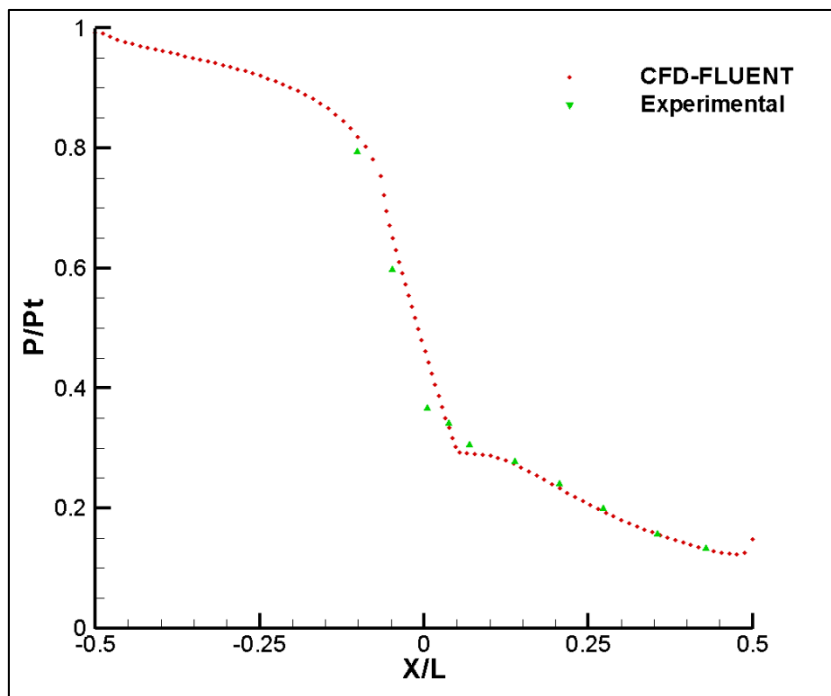
Figure 28 Results of Wall Pressure Ratio Nozzle B$_3$
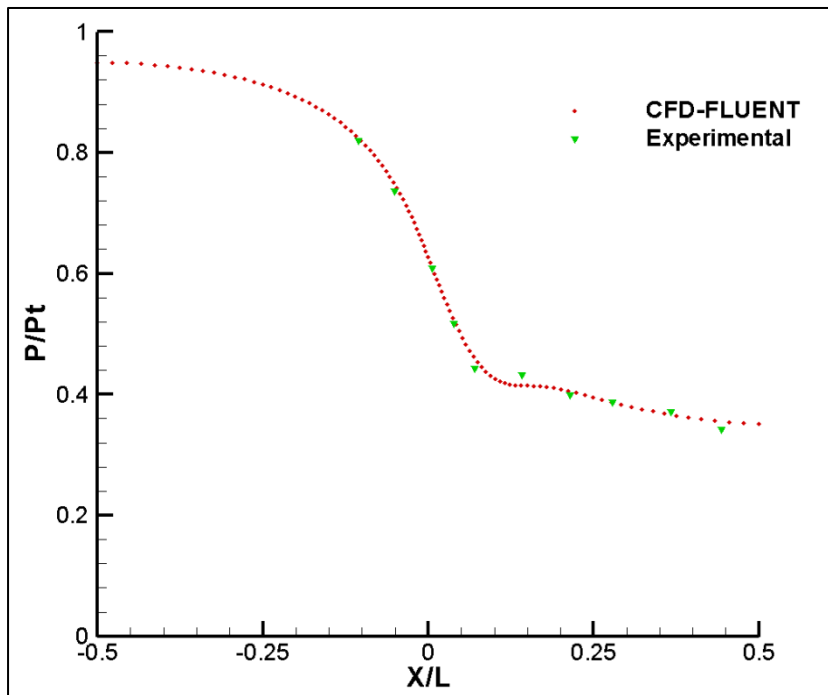
Figure 29 Results of Centerline Pressure Ratio Nozzle A$_1$
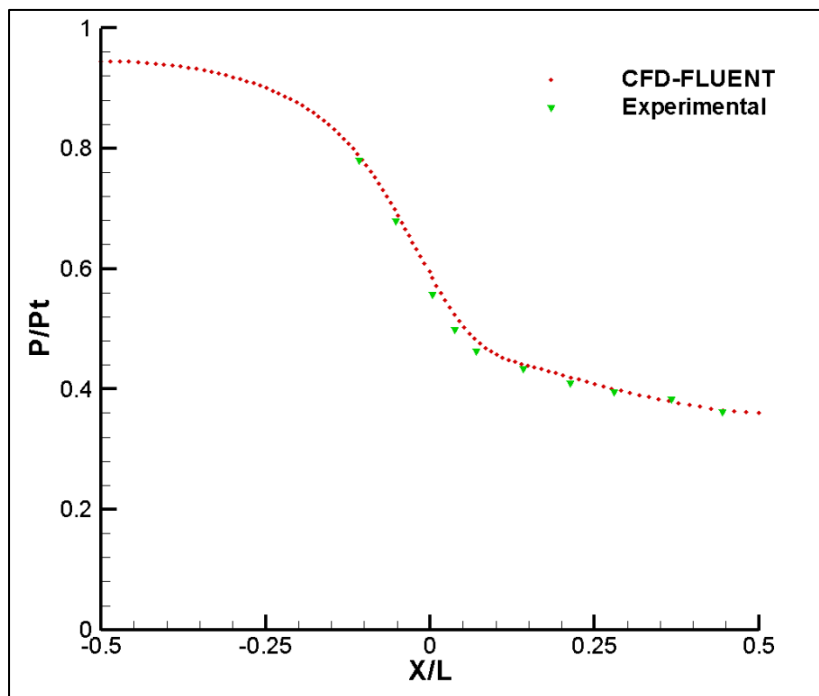
Figure 30 Results of Centerline Pressure Ratio Nozzle A$_2$
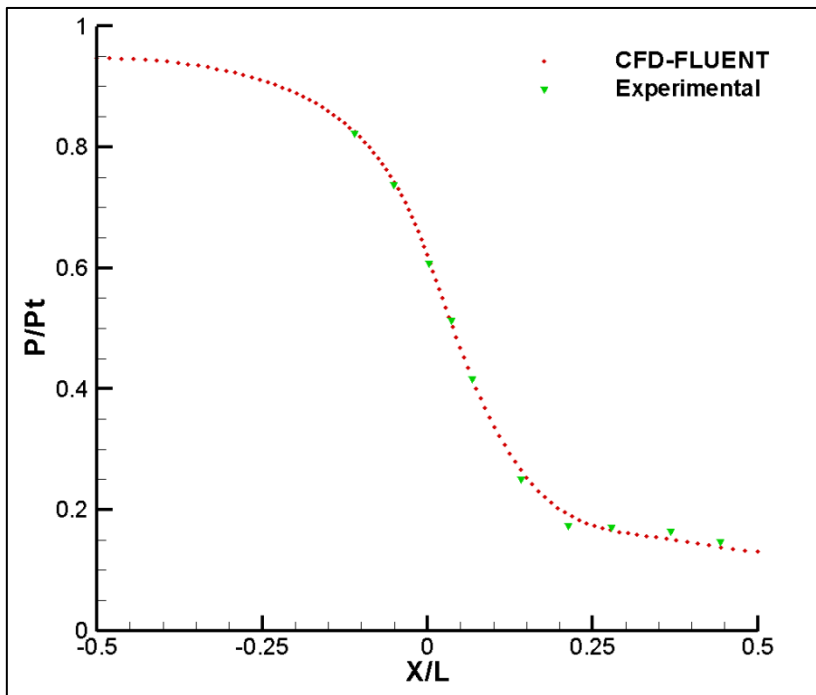
Figure 31 Results of Centerline Pressure Ratio Nozzle B₁
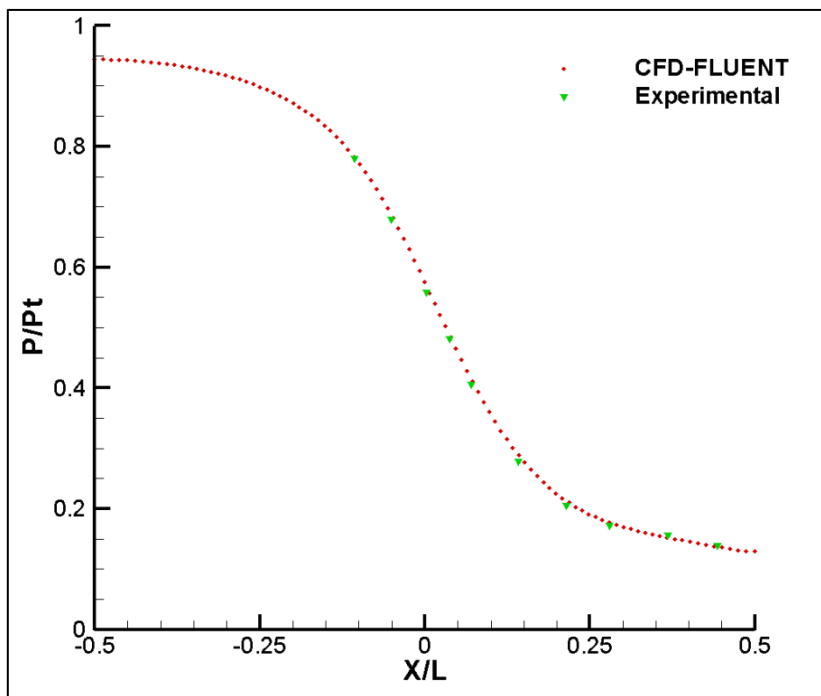
Figure 32 Results of Centerline Pressure Ratio Nozzle B₂
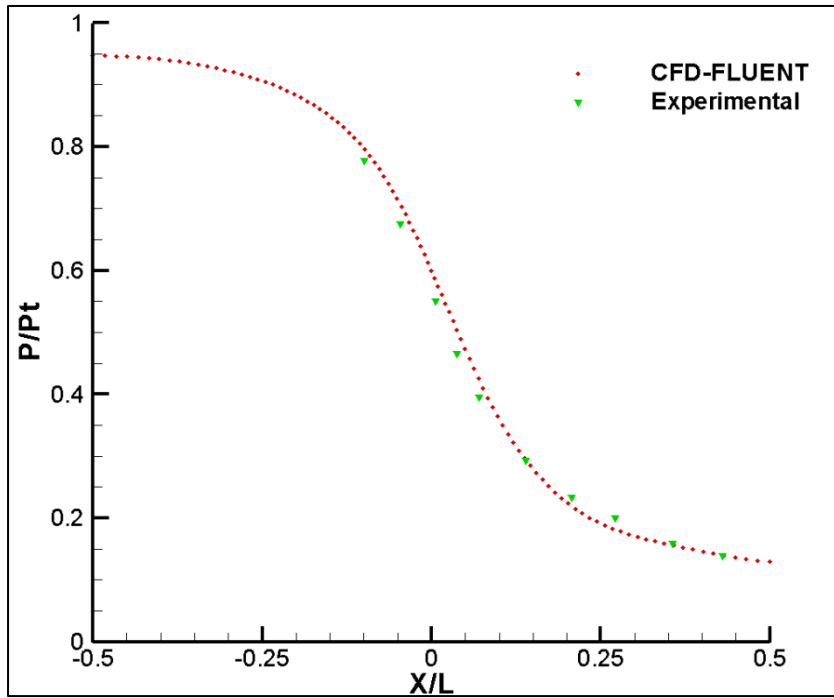
Figure 33 Results of Centerline Pressure Ratio Nozzle B$_3$

In cases A1 and A2, the computational solution accurately estimates the experimental data although there are some slight discrepancies in the downstream of nozzle throat; see Figure 24, Figure 25 . In the case of supersonic flow at the nozzle exit the pressure ratio will not affect the wall pressure ratio which also can be interpreted form the experimental data [12]. Wall pressure ratio and centerline pressure ratio evaluated from the solver match almost perfectly with experimental data. The similar behaviors are also observed in Figures 4 –13. Furthermore above results also indicate the internal performance of the nozzles with respect to throat area yet it will not be discussed in this study [8].

CHAPTER 3

STRUCTURAL ANALYSIS

As the scope of the study; the effects of static aeroelasticity on the nozzle performance will be investigated. The results evaluated with the rigid and flexible nozzle wall assumptions will be compared. In the flexible wall model, the nozzle wall is assumed to be cantilevered at the nozzle inlet. The nozzle material is selected as aluminum. By assuming the flexible walls are 2D linear beam elements; displacements in the nozzle wall are calculated.

3.1. BEAM ELEMENTS

The beam element is assumed to be linear bar of uniform cross section capable of resisting axial forces, bending moments about the two principal axes in the plane of its cross section, and twisting moments about its centric axis. Beam element has 6 degree of freedom at each node. Figure 34 represents a beam element with 6 degree of freedom at the node j.
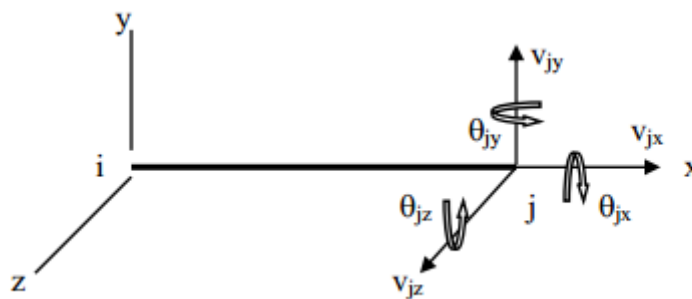
Figure 34 Beam Element with 6 D.O.F

3.2. ELEMENT STIFFNESS MATRIX

Two-dimensional beam element with three displacement degrees of freedom at each end of beam will be considered as it is illustrated in Figure 35. The degrees of freedom are axial deflections d_1^l and d_4^l, transverse deflections d_2^l and d_5^l, rotations d_3^l and d_6^l at the each end of beam element. Local coordinate is denoted by x^l, y^l. The length of beam element is given by l_b and thickness is t_b. The forces acting on the beam element are f_n where $n = 1...6$ and correspond at the same direction as displacements. Local coordinate and global coordinate system, degrees of freedom for two nodes can be seen also in Figure 35.
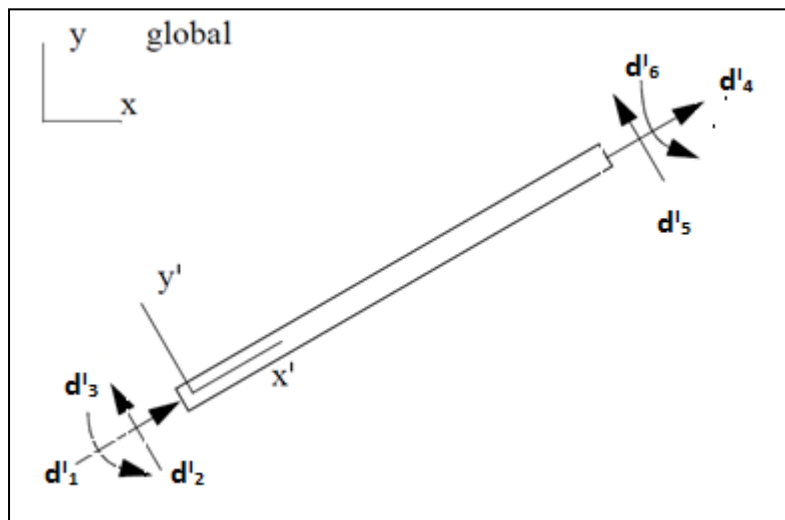
Figure 35 2-D Linear Beam Element

There are six possible degrees of freedom in each beam element; hence the displacements are determined by 6×6 element stiffness matrix k_e^l. Displacements are considered as positive in the direction of the coordinate axis. Therefore for the element above;

$$\{f^l\} = [k^l]\left[d^l\right]$$ 4.2.1

where

$$\{f^l\} = \begin{bmatrix} f_1{}^l \\ f_2{}^l \\ f_3{}^l \\ f_4{}^l \\ f_5{}^l \\ f_6{}^l \end{bmatrix} \quad and \quad \{d^l\} = \begin{bmatrix} d_1{}^l \\ d_2{}^l \\ d_3{}^l \\ d_4{}^l \\ d_5{}^l \\ d_6{}^l \end{bmatrix}$$

Direct integration of the governing differential equations for axial and transverse deformation will yield the element stiffness matrix [13]. Hence the element stiffness matrix is;

$$[k_e^l] = \begin{bmatrix} \dfrac{AE}{L} & 0 & 0 & -\dfrac{AE}{L} & 0 & 0 \\[2mm] 0 & \dfrac{12EI}{L^3} & \dfrac{6EI}{L^2} & 0 & -\dfrac{12EI}{L^3} & \dfrac{6EI}{L^2} \\[2mm] 0 & \dfrac{6EI}{L^2} & \dfrac{4EI}{L} & 0 & -\dfrac{6EI}{L^2} & \dfrac{2EI}{L} \\[2mm] -\dfrac{AE}{L} & 0 & 0 & \dfrac{AE}{L} & 0 & 0 \\[2mm] 0 & -\dfrac{12EI}{L^3} & -\dfrac{6EI}{L^2} & 0 & \dfrac{12EI}{L^3} & \dfrac{6EI}{L^2} \\[2mm] 0 & \dfrac{6EI}{L^2} & \dfrac{2EI}{L} & 0 & -\dfrac{6EI}{L^2} & \dfrac{4EI}{L} \end{bmatrix}$$ 4.2.2

The axial area for a two dimensional beam element is equal to beam thickness. And the moment of inertia is $th^3/12$ for rectenguar shape and $\pi(r_o^4 - r_i^4)/4$ for an annulus. The elements equations are stated in the given local element coordinate system. To couple the equations from all beam elements, each equation needs to be transferred into a global coordinate system. Coordinate transformation is required to proceed and the relation is given in Figure 36.
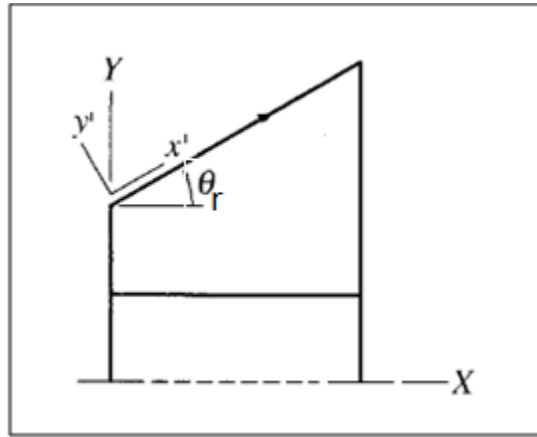
Figure 36 Local and Global Coordinates

The relation between local and global coordinate system can be written by transformed the axis by angle of θ_r. The detail work of obtaining transformation matrix and stiffness matrix is explained in Przemieniecki [13]. Therefore the transformation matrix will be a 6×6.

$$[T] = \begin{bmatrix} \cos\theta_r & \sin\theta_r & 0 & 0 & 0 & 0 \\ -\sin\theta_r & \cos\theta_r & 0 & 0 & 0 & 0 \\ 0 & 0 & 1 & 0 & 0 & 0 \\ 0 & 0 & \cos\theta_r & \sin\theta_r & 0 & 0 \\ 0 & 0 & -\sin\theta_r & \cos\theta_r & 0 & 0 \\ 0 & 0 & 0 & 0 & 0 & 1 \end{bmatrix} \qquad 4.2.3$$

Simply the rotation angles of each element can be computed form node points. Hence the member direction cosines;

$$\cos\theta_r = \frac{X_2 - X_1}{\sqrt{(X_2 - X_1)^2 + (Y_2 - Y_1)^2}} \quad , \quad \sin\theta_r = \frac{Y_2 - Y_1}{\sqrt{(X_2 - X_1)^2 + (Y_2 - Y_1)^2}} \qquad 4.4.4$$

Since the transformation matrix is symmetric $[T]^T = [T]^{-1}$. The transformation of the local stiffness matrices into global stiffness matrices;

$$[k_e] = [T]^T [k_e'][T] \qquad 4.4.5$$

Then the equation *4.a.1*;

$$[T]^T \{f^I\} = [T]^T [k^I][T][T]^T [d^I]$$ 4.4.6

The governing equation of the direct stiffness method can be written as;

$$\{f_G\} = [K_G][d_G]$$ 4.4.7

The contribution of each beam element should be included in the global stiffness matrix. For instance consider 2 beam elements as illustrated in **Hata! Başvuru kaynağı bulunamadı.**.
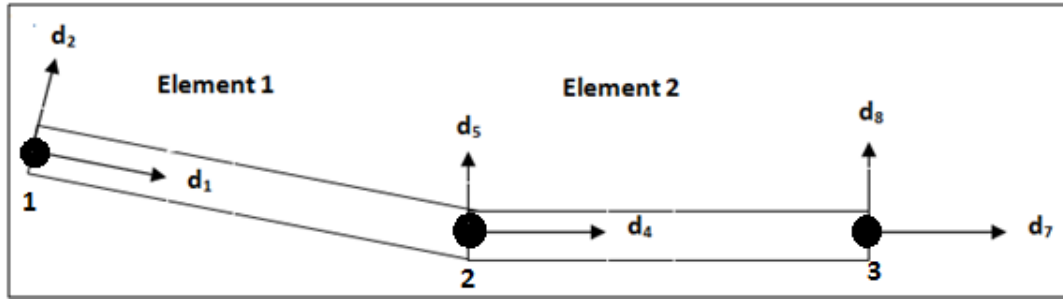
Figure 37 Two Beam Element Structure

Creating each beam stiffness matrix;

$$[k_e^1] = \begin{bmatrix} k_{11}^1 & k_{12}^1 & k_{13}^1 & k_{14}^1 & k_{15}^1 & k_{16}^1 \\ k_{21}^1 & k_{22}^1 & k_{23}^1 & k_{24}^1 & k_{25}^1 & k_{26}^1 \\ k_{31}^1 & k_{32}^1 & k_{33}^1 & k_{34}^1 & k_{34}^1 & k_{36}^1 \\ k_{41}^1 & k_{42}^1 & k_{43}^1 & k_{44}^1 & k_{45}^1 & k_{46}^1 \\ k_{51}^1 & k_{52}^1 & k_{53}^1 & k_{54}^1 & k_{55}^1 & k_{56}^1 \\ k_{61}^1 & k_{62}^1 & k_{63}^1 & k_{64}^1 & k_{65}^1 & k_{66}^1 \end{bmatrix}, [k_e^2] = \begin{bmatrix} k_{11}^2 & k_{12}^2 & k_{13}^2 & k_{14}^2 & k_{15}^2 & k_{16}^2 \\ k_{21}^2 & k_{22}^2 & k_{23}^2 & k_{24}^2 & k_{25}^2 & k_{26}^2 \\ k_{31}^2 & k_{32}^2 & k_{33}^2 & k_{34}^2 & k_{34}^2 & k_{36}^2 \\ k_{41}^2 & k_{42}^2 & k_{43}^2 & k_{44}^2 & k_{45}^2 & k_{46}^2 \\ k_{51}^2 & k_{52}^2 & k_{53}^2 & k_{54}^2 & k_{55}^2 & k_{56}^2 \\ k_{61}^2 & k_{62}^2 & k_{63}^2 & k_{64}^2 & k_{65}^2 & k_{66}^2 \end{bmatrix}$$

The element stiffness matrix for element 1 is stored in the portion of the global stiffness matrix that involves nodes 1 and 2. In the same manner nodes 2 and 3 has been stored in 6×6 matrix. So running the stiffness matrix builder code, construction of global stiffness matrix of two beam elements can be given as;

$$
[k] = \begin{bmatrix}
k_{11}^1 & k_{12}^1 & k_{13}^1 & k_{14}^1 & k_{15}^1 & k_{16}^1 & 0 & 0 & 0 \\
k_{21}^1 & k_{22}^1 & k_{23}^1 & k_{24}^1 & k_{25}^1 & k_{26}^1 & 0 & 0 & 0 \\
k_{31}^1 & k_{32}^1 & k_{33}^1 & k_{34}^1 & k_{34}^1 & k_{36}^1 & 0 & 0 & 0 \\
k_{41}^1 & k_{42}^1 & k_{43}^1 & k_{44}^1+k_{11}^2 & k_{45}^1+k_{12}^2 & k_{46}^1+k_{13}^2 & k_{14}^2 & k_{15}^2 & k_{16}^2 \\
k_{51}^1 & k_{52}^1 & k_{53}^1 & k_{54}^1+k_{21}^2 & k_{55}^1+k_{22}^2 & k_{56}^1+k_{23}^2 & k_{24}^2 & k_{25}^2 & k_{26}^2 \\
k_{61}^1 & k_{62}^1 & k_{63}^1 & k_{64}^1+k_{31}^2 & k_{65}^1+k_{32}^2 & k_{66}^1+k_{33}^2 & k_{34}^2 & k_{34}^2 & k_{36}^2 \\
0 & 0 & 0 & k_{41}^2 & k_{42}^2 & k_{43}^2 & k_{44}^2 & k_{45}^2 & k_{46}^2 \\
0 & 0 & 0 & k_{51}^2 & k_{52}^2 & k_{53}^2 & k_{54}^2 & k_{55}^2 & k_{56}^2 \\
0 & 0 & 0 & k_{61}^2 & k_{62}^2 & k_{63}^2 & k_{64}^2 & k_{65}^2 & k_{66}^2
\end{bmatrix}
$$

The same procedure can be applied for all beam elements. Since we analyzed our case with 100 grid points in stream-wise direction we have 100 linear beam elements. Each of two nodal points creates a beam element. The loading on the finite elements is not discrete. Each element, which is also a beam element, will be subjected to distributed pressure load which is equal to flow static pressure and a distributed shear load equal to viscous wall shear stress. Consistency will be provided by assuming loads are constant along the length of the beams. So for two element beam the structural system to be solved becomes;

$$
\begin{bmatrix}
f_1 \\ f_2 \\ f_3 \\ f_4 \\ f_5 \\ f_6 \\ f_7 \\ f_8 \\ f_9
\end{bmatrix} =
\begin{bmatrix}
k_{11}^1 & k_{12}^1 & k_{13}^1 & k_{14}^1 & k_{15}^1 & k_{16}^1 & 0 & 0 & 0 \\
k_{21}^1 & k_{22}^1 & k_{23}^1 & k_{24}^1 & k_{25}^1 & k_{26}^1 & 0 & 0 & 0 \\
k_{31}^1 & k_{32}^1 & k_{33}^1 & k_{34}^1 & k_{34}^1 & k_{36}^1 & 0 & 0 & 0 \\
k_{41}^1 & k_{42}^1 & k_{43}^1 & k_{44}^1+k_{11}^2 & k_{45}^1+k_{12}^2 & k_{46}^1+k_{13}^2 & k_{14}^2 & k_{15}^2 & k_{16}^2 \\
k_{51}^1 & k_{52}^1 & k_{53}^1 & k_{54}^1+k_{21}^2 & k_{55}^1+k_{22}^2 & k_{56}^1+k_{23}^2 & k_{24}^2 & k_{25}^2 & k_{26}^2 \\
k_{61}^1 & k_{62}^1 & k_{63}^1 & k_{64}^1+k_{31}^2 & k_{65}^1+k_{32}^2 & k_{66}^1+k_{33}^2 & k_{34}^2 & k_{34}^2 & k_{36}^2 \\
0 & 0 & 0 & k_{41}^2 & k_{42}^2 & k_{43}^2 & k_{44}^2 & k_{45}^2 & k_{46}^2 \\
0 & 0 & 0 & k_{51}^2 & k_{52}^2 & k_{53}^2 & k_{54}^2 & k_{55}^2 & k_{56}^2 \\
0 & 0 & 0 & k_{61}^2 & k_{62}^2 & k_{63}^2 & k_{64}^2 & k_{65}^2 & k_{66}^2
\end{bmatrix}
\begin{bmatrix}
d_1 \\ d_2 \\ d_3 \\ d_4 \\ d_5 \\ d_6 \\ d_7 \\ d_8 \\ d_9
\end{bmatrix}
$$

The steps of procedures can be summarized as follows:

- Build the element stiffness matrix in local coordinates.
- Transform the element stiffness matrix into global coordinate system
- Construct the global stiffness matrix using transformed element stiffness matrices
- Reduce the global stiffness matrix by applying the boundary constraints and solution of nodal displacement.

The stiffness matrix **K** in a typical finite problem can be characterized as symmetric, sparse, and band structured. Figure 38 illustrates a sample of banded sparse matrix which can be stored and factored efficiently. Stiffness matrix builder code has been developed in order to create the structural system. Computed and constructed stiffness matrix portion of the case studies is presented in Figure 39.

$$[K] = \begin{bmatrix}
x & x & & x & & & & & & & & & \\
x & x & x & & x & & & & & & & & \\
 & x & x & x & & x & & & & & & & \\
x & & x & x & x & x & & & & & & & \\
 & x & & x & x & x & x & & & & & & \\
 & & x & x & x & x & x & & x & & & & \\
 & & & x & x & x & x & & x & & & & \\
 & & & & x & x & x & & & x & & & \\
 & & & x & & x & x & x & x & & & \\
 & & & x & & x & x & x & x & \\
 & & & & x & x & x & x & x & \\
 & & & & & x & x & x & \\
 & & & & & & . & & & & & & \\
\end{bmatrix}$$

Figure 38 A Banded Matrixes with Nonzero Terms

Figure 39 Portion of Constructed Stiffness Matrix of Many Elements

3.3. FORCE VECTOR

The force acting on the finite portion of the structure is not discrete. It is continuous along the element. Each volume of a flow boundary is under a distributed pressure force which is actually static pressure. And addition to static pressure the element also subjected to shear force which is indeed viscous wall shear stress. The loads in this case are assumed to be constant along each element. To begin with; for the axial and transverse deflections:

$$L_1 = 1 - x^t / le \qquad\qquad 4.7.6$$

$$L_2 = x^t / le \qquad\qquad 4.7.7$$

$$f_1 = \int_0^{le} \tau_w L_1 dx^t \qquad\qquad f_2 = \int_0^{le} \tau_w L_2 dx^t \qquad\qquad 4.7.8$$

$$L_2 = 1 - 3(\frac{x^t}{le})^2 + 2(\frac{x^t}{le})^3 \qquad\qquad 4.7.9$$

$$L_3 = le\left(\frac{x^t}{le} - 2(\frac{x^t}{le})^2 + (\frac{x^t}{le})^3 \right) \qquad\qquad 4.7.10$$

$$L_5 = 3(\frac{x^t}{le})^2 - 2(\frac{x^t}{le})^3 \qquad\qquad 4.7.11$$

$$L_3 = le\left(-(\frac{x^t}{le})^2 + (\frac{x^t}{le})^3 \right) \qquad\qquad 4.7.12$$

So the forces acting on a linear beam element [12], [14];

36

$$f_1 = \frac{\tau_w le}{2} \ , f_2 = \frac{Ple}{2} \ , f_3 = \frac{Ple^2}{12} \ , f_4 = \frac{\tau_w le}{2}, f_5 = \frac{Ple}{2}, f_6 = -\frac{Ple^2}{12} \qquad 4.7.13$$

Elements shape functions and Hermite cubic result in equation 4.7.13 for one node in beam element. Concentrated force due to surface pressure can be determined accordingly for many elements in a continuous structure.

CHAPTER 4

# NOZZLE PERFORMANCE CHANGE

4.1. FEXIBLE WALL GEOMETRY CHANGE

In the case of 2D flexible wall; the nozzle walls are assumed to be cantilevered at the nozzle inlet and they are free from the nozzle outlet. Material is selected to be aluminum for the flexible walls. The value of Young's modules is chosen accordingly. Thickness of the rectangular and circular beam elements is chosen to be 3 mm and 6 mm to see the effect of flexibility by thickness also. Loose-coupled method has been used to carry the problem solution. Furthermore to be more realistic, the solution case also solved as axisymmetric problem and compared with 2D cases. Flow solution and structure solution is obtained simultaneously. Figure 40, Figure 41, Figure 42 presents and gives the results of the effect of flexibility on nozzle wall geometry of B_2 for different wall thicknesses. As it was expected the high pressure inside the nozzle will deform the wall geometry towards outward. Since the nozzle inlet is fixed there is no deformation and the geometry stays as it was and the wall deformation increases in a manner such that the highest deformation will be at the nozzle exit. The effect of wall thickness is also can be obtained from the results. As the wall thickness increases the stiffness of the wall will increase and cause less deflection. The stiffness matrix is highly dependent on the element thickness. Moreover selected material is also an important parameter for stiffness matrix. The material used to construct the nozzle wall is Aluminum. Changing the material to more rigid like steel or more flexible material will also give a significant effect on stiffness matrix. Stiffness matrix is a direct way to change the deflections size.
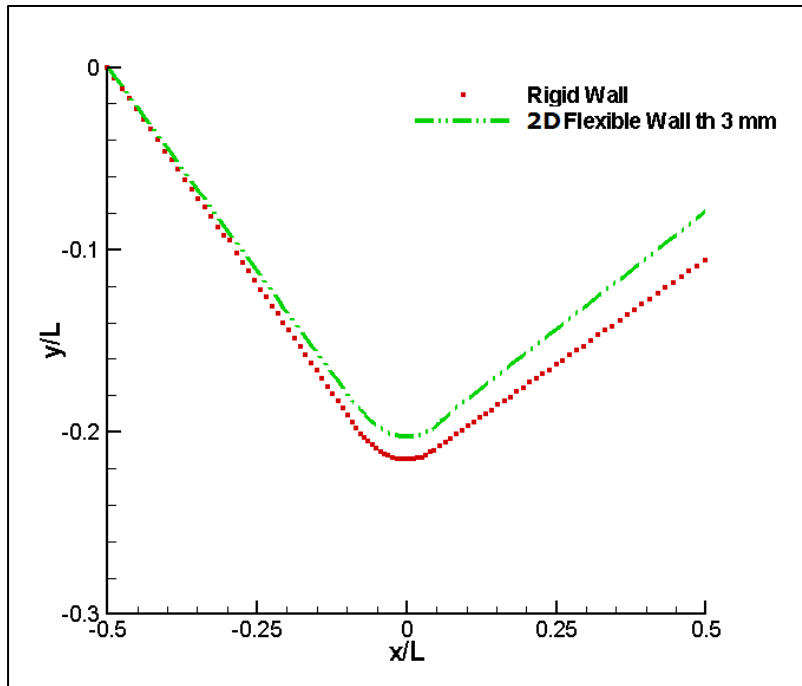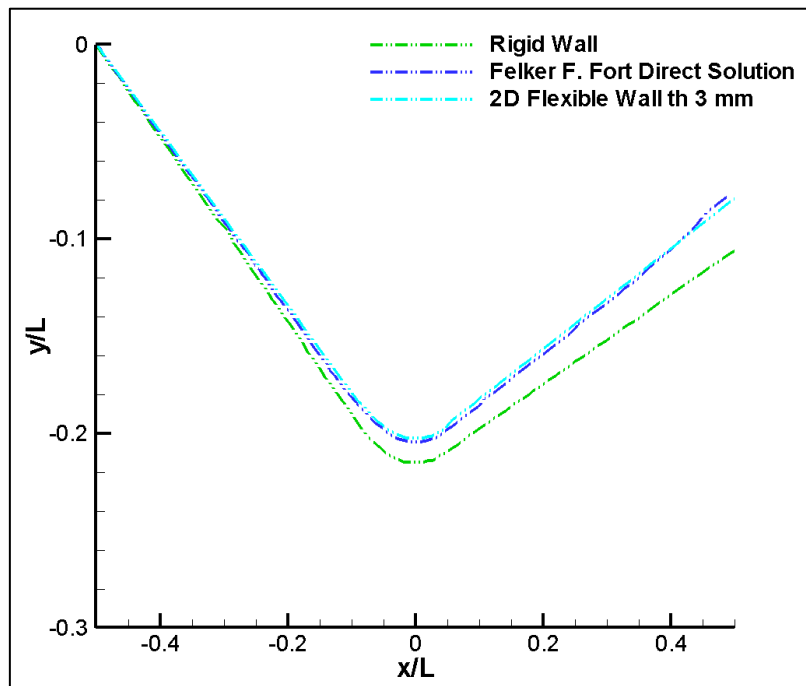
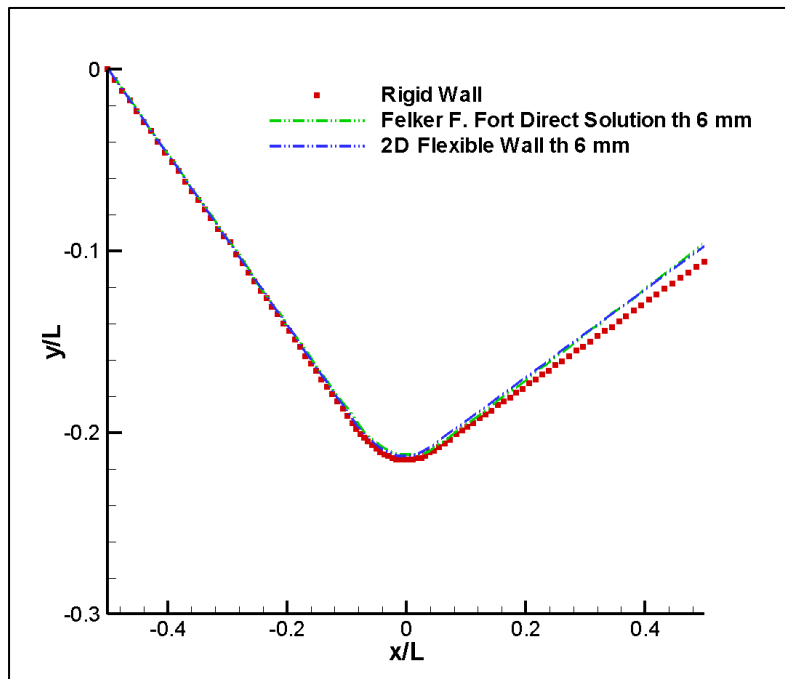**Figure 40 Rigid Nozzle Wall vs. Flexible Nozzle Wall Geometry-Nozzle B$_2$**
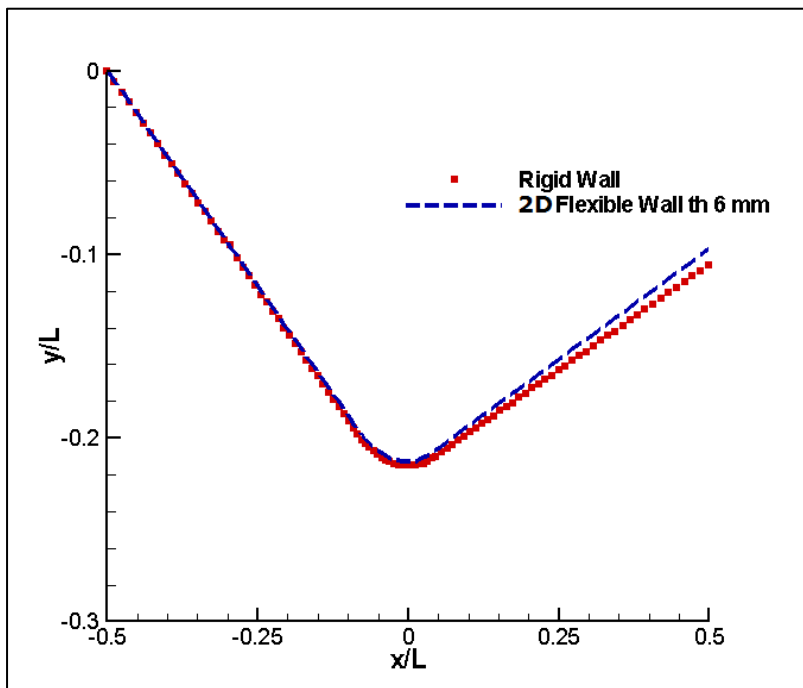
Figure 41 Rigid Nozzle Wall vs. Flexible Nozzle Wall Geometry-Nozzle B$_2$
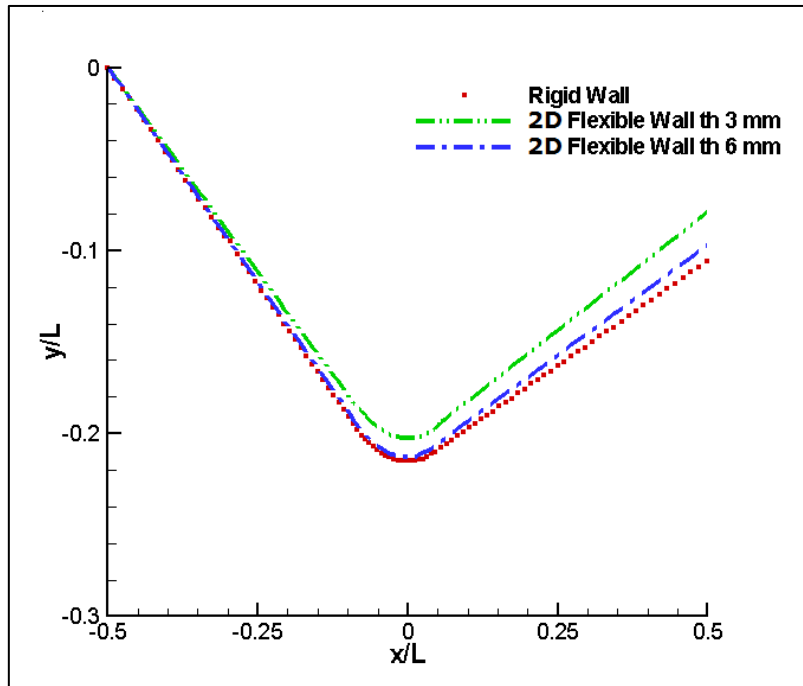
Figure 42 Rigid Nozzle Wall vs. Flexible Nozzle Wall Geometry-Nozzle B₂

Figure 43 Comparisons of The Results with Direct Solution of Felker F. Fort-Nozzle B₂, th 3 mm

Figure 44 Comparisons of The Results with Direct Solution of Felker F. Fort-Nozzle B$_2$,th 6mm

Figure 43 and Figure 44 illustrates the comparisons of the 2D Flexible Wall results with Felker F. Fort direct solution [5] [12] for both thicknesses; 3mm and 6 mm. After the first iteration is completed the new geometry reanalyzed. In the second iteration the walls almost had no deformation due to pressure differences occurred was small and so the convergence obtained by then. Solutions obtained for axisymmetric case are compared with rigid walls, 2D case results and Felker. F. Fort [5][12]. In the case of axisymmetric, the beam elements are modeled as circular hallow elements and the stiffness matrixes for the case is obtained accordingly [15]. The main change in the stiffness matrix is done due to inertia change. This change creates us more stiff elements and the results of more stiff elements indicate that the existing geometry will deform less than the 2D case. In both results show us the consistency with the model assumptions and results give good approximation to the Felker. F. Fort results. Figure 45 and Figure 46 present the results obtained for all cases. Consistency and accuracy of the results with each other has been provided

42

almost perfectly. In the axisymmetric case since the geometry is stiffer, deformation obtained less according to 2D case.
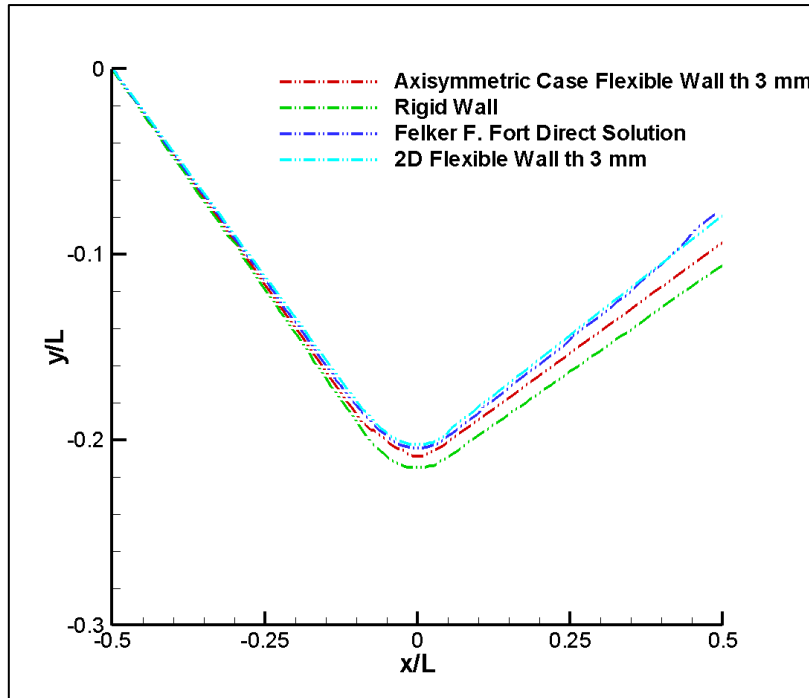

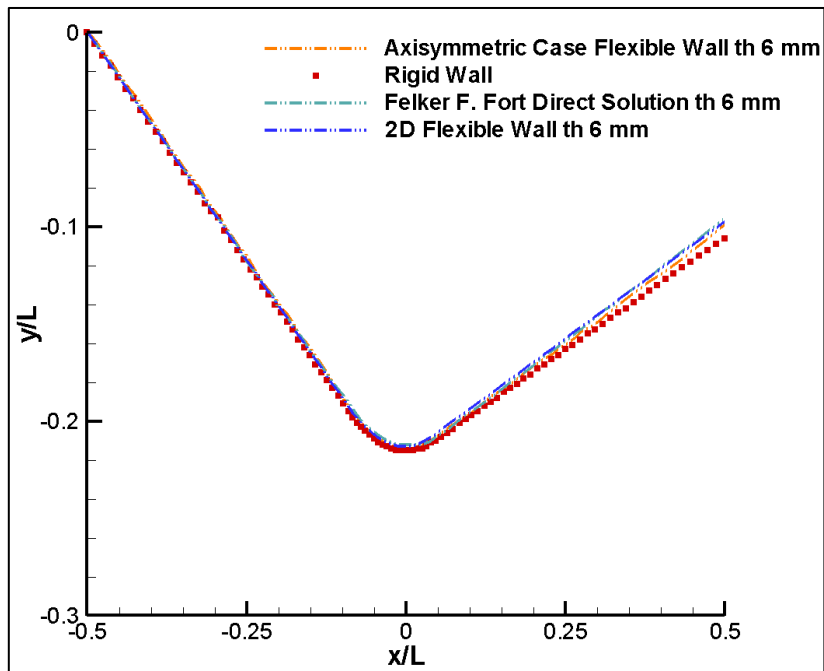**Figure 45 Comparisons of All Cases for th 3 mm**

Figure 46 Comparisons of All Cases for th 6 mm

4.2. NOZZLE PERFORMANCE by FEXIBLE WALL GEOMETRY CHANGE

In all cases, the performance change due to wall flexibility is presented in Figure 47 and Figure 48. Remarkable effect on flow characteristic due to geometry change can be seen clearly from the results. Mach number changes in a favorable manner. The nozzle expansion ratio increases as the wall deflects. This may be a desired result and affects our performance in positive manner. The increase of expansion ratio may give favorable result up to a point. There exists only one expansion ratio that optimizes the whole performance of the nozzle. The expansion ratio that maximizes the performance will be affected due the wall flexibility. Static pressure drops as the deflection increases. Moreover deflection of the nozzle wall outward increases the divergence angle. Thus the effects should be considered while designing a nozzle. Consideration of pressure drop, mass flow rates, Mach number altering should be taken into account in existence of aeroelasticity and its flexibility.
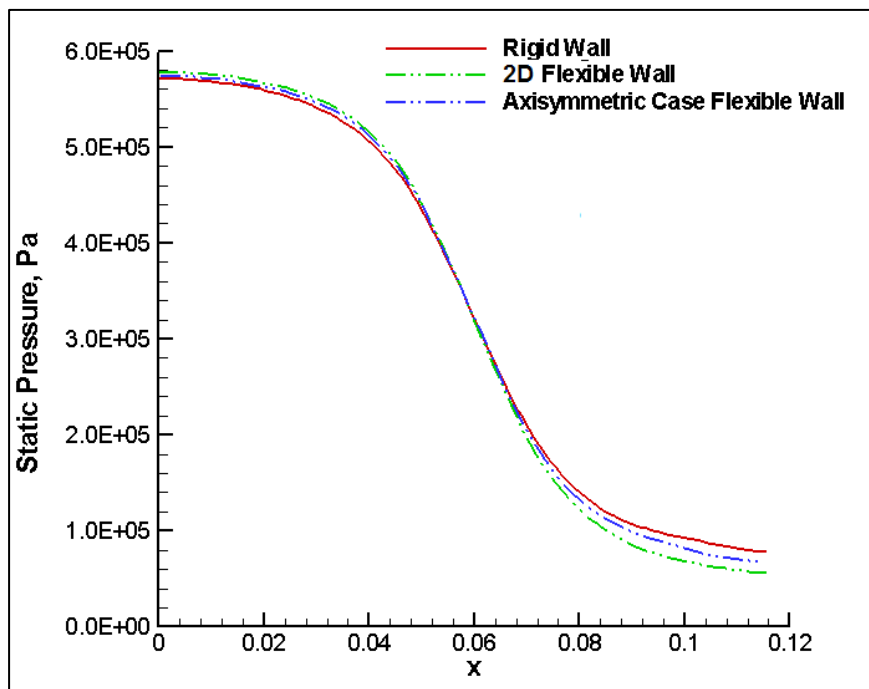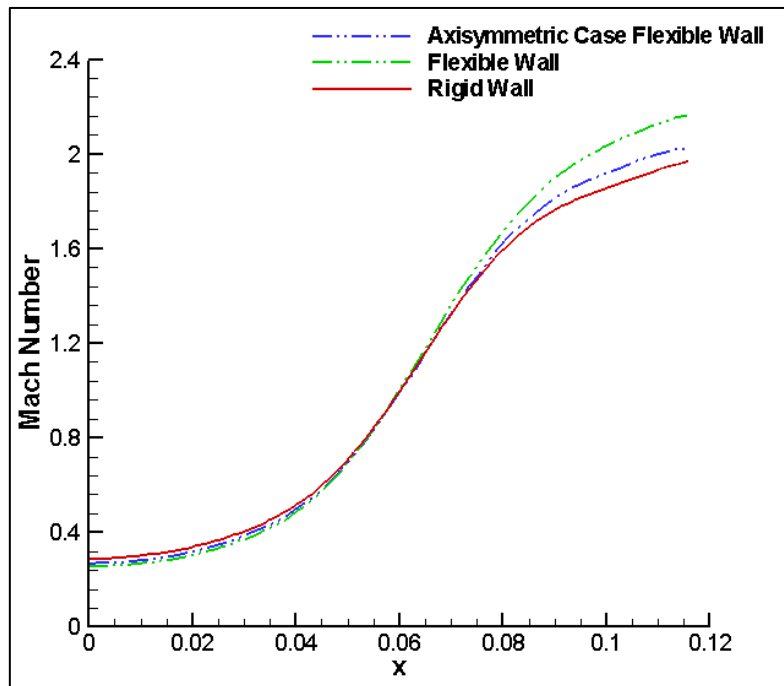

Figure 47 Comparison of Static Pressure of Nozzle B$_2$, Flexible Wall Cases and Rigid Wall, th 3 mm

Figure 48 Mach number of Nozzle B$_2$ with Flexible Wall Cases and Rigid Wall , th 3 mm

The difference between the internal pressure and exit pressure directly affect the wall deflections. The deflection is proportional to the pressure differences. Pressure differences will directly change the pressure ratio and may change trust ratio which is a function of pressure ratio. Obviously, high pressure ratio will generate high loads and causes larger wall deflections. The flexibility is also proportional with structure stiffness. Reducing the material stiffness will yield larger deflections. Determining for a material will be a concern under flexibility case. The capability of the analysis conducted shows the importance of the aeroelastic effect and nozzle performance response. The results above give a better understanding on the behavior of structure under aerodynamic load in nozzles. A supersonic compressible fluid interacting with nozzle body results in change of whole body. While the deformation takes place, the throat area of the nozzle also deforms and updates to new nozzle which is totally different from previous nozzle. As it is presented in Chapter 2, nozzle performance significantly changes with nozzle throat area. The aerodynamic

optimization should consider the aeroelastic analysis accordingly. The new aerodynamic shape will also affect the mass flow rate of the nozzles. The mass flow rate will be determined by narrowest cross sectional area of the nozzle keeping velocity constant. The results above indicate that the nozzle is under aeroelastic case which will yield a significant amount of side loads. Nozzle throat variation will also yield a new side loads. One of the main reasons of side loads is the aeroelastic interaction between wall pressure and structure stiffness. The aeroelastic analysis needs deep consideration so that the side loads can be obtained effectively. As the figures above shows, considering the wall displacement to determine the pressure acting in the nozzle and the performance is very important and this is one of the scope points of this thesis. These above preliminary results suggest that aeroelastic effects should not be ignored, over passed in the phase of design or analysis of converging-diverging supersonic nozzles, and that strict design approaches that do not directly account for aeroelastic effects could fall in a substantial failures.

CHAPTER 5

CONCLUSIONS and FUTURE WORK

5.1.CONCLUSIONS

In this thesis, the effect of static aeroelasticity on two-dimensional converging diverging nozzle has been analyzed and demonstrated. The methodology studied is used to investigate the fluid-dynamic and aeroelastic behavior in converging-diverging nozzle geometry. Five different nozzle configurations have been selected and flow analysis has been performed by using commercial CFD package code. The commercial CFD package code then has been validated by comparing the CFD results with experimental data. Flow analyses results lead us to perform structural analysis to the nozzle wall and observe the wall flexibility. One of the five configurations, nozzle B_2, has been selected to analyze its wall flexibility under the aerodynamic loads. Direct stiffness method has been used to determine the wall deflections. The methodology of a two-way loose-coupling between an accurate CFD solver and direct stiffness method is used. Thus, nozzle B_2 then has been reanalyzed with deflected wall to see the performance change. Results show us considerably significant effect of static aeroelasticity on the nozzle performance. Firstly, the amount of deflection under existing aerodynamic load is depended on the material used and nozzle wall thickness. Those parameters will directly affect the stiffness of the structure. Secondly, the flexibility of the wall will change the nozzle performance. Results indicate that once the wall deflected, the expansion ratio will increase which seems a favorable and pressure will decrease. However as an effect of aeroelasticity, designer should take into account that the expected performance may alter due to the flexibility. Expected performance under rigid wall differs from the performance of flexible wall. Parameters such as nozzle

wall material and nozzle wall thickness should be selected for optimum design. Selecting less stiff material will lead in light nozzles. Although you lose weight which is desired for whole system, you lose strength which needs consideration under existing loads.

In conclusion, in the design phase of a nozzle, the effect of aeroelasticity should be considered. Since there will exist only one expansion ratio that optimizes the whole performance of the nozzle, designer should think and take a consideration on changing of the expansion ratio due to the flexible wall. In the design phase material selection, wall thickness parameters should be determined by taking account of aeroelastic effects.

5.2.FUTURE WORK

Methodology to determine desired aerodynamic shape and performance can be developed by further consideration. The preliminary summaries obtained in this work can surely be strengthened, forwarded with longer run times and with adding more computational results covering a wide range of pressure ratios. Effects and results of aeroelasticity can be implemented in the optimization of aerodynamic shapes. Direct solution technique can be developed to solve both fluid and structural dynamics while interacts each other. Validation of the aeroelastic effect can be conducted with test setup which will require great effort to build up. Addition to static aeroelasticity, unsteady, modal phenomena can be investigated and a model can be developed in this manner which I desire to investigate in my post-degrees.

REFERENCES

[1] R.M. Kolonay , *Computational Aeroelasticity*, The Applied Vehicle Technology Panel, General Electric Corporate Research & Development Center, Ankara, 2001

 [2] Mason, D. , R. , Blotter, P., R. , "*Finite Element Application to Rocket Nozzle Aeroelasticity*" J. Propulsion, Vol.2, No. 6, November-December, 1986

[3] Karpel, M., Yaniv, S. , Livshits, D. , S. , "*Integrated Solution for Computational Static Aeroelasticity*" Journel of Spacecraft and Rockets, Vol. 35, No. 5, September-October, 1998

 [4] Harkins, T. K., Courter, R. W., "*Aeroelastic Effects on Range-Acquired Aerodynamic Coefficients*", AIAA-90-0082, Louisiana, 1990

[5] Felker, F., F., "*A New Method for Transonic Static Aeroelasticity Problems*" , AIAA-92-2123, NASA Ames Research Center, California, 1992

[6] Zhao, X., Bayyuk, S., Zhang, S. , "*Aeroelastic Response of Rocket Nozzles to Asymmetric Thrust Loading*" Elsevier, May 2012

[7] Garelli, L., Paz, R. R., Storti, A. M. , "*Fluid-Structure Interaction Study of The Start-up a Rocket Enginee Nozzle*" INTEC, May,2009

[8] Mason, M. , L. , Putnam, L. , E. , "*The Effect of Thoat Contouring on Two-Dimensional Converging-Diverging Nozzles at Static Conditions*", NASA technical paper, August 1980

[9] Capone, F., J., Bangert, S., Asbury, S., C., Mills, C., T., L., Bare, E., A.,"*The NASA Langley 16-Foot Transonic Tunnel: Historical Overview, Facility Description, Calibration, Flow Characteristics, and Test Capabilities*" NASA technical paper 3521, September 1995

[10] Chorin, A., J. , "*Numerical solution of Navier-Stokes equations. Mathematics of Computation*", 22:745-762, 1968.

[11] FLUENT user's guide, September 2006

[12] Felker, F. , F. , " *Direct Solutions of the Navier-Stokes Equations with application to static aeroelasticity*", 1982, Stanford University.

[13] Przemieniecki, J. ,S. , "*Theory of Matrix Structural Analysis*" 5.6: 70-71, Newyork 1968, McGraw-Hill

[14] Meirovitch, L., "*Elements of Vibration Analysis*" McGraw-Hill, NewYork, 1975

[15] Witmer, E., A., Kotanchik, J., J., "*Progress Report On Discrete-Element Elastic and Elastic-Plastic Analysis of Shells of Revolution Subjected To Axisymmetric and Asymmetric Loading*", MIT, AFFDL-TR-68-150

APPENDIX A

TEST RESULTS OF NOZZLE CONFIGURATIONS by THE LANGLEY 16-FOOT TRANSONIC TUNNEL

The comparison plots for two-dimensional, inviscid theory model with experimental data are stated below [8].
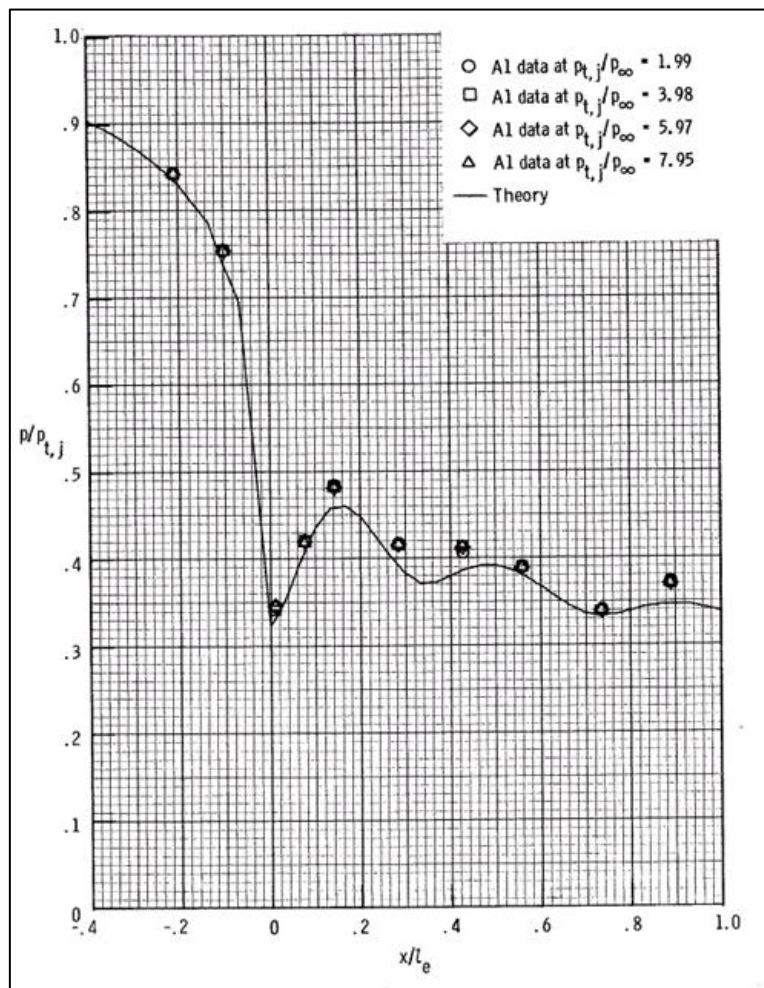
Figure A.1 Comparison of Theoretical and Experimental Static-Pressure Distributions on Center Line for Nozzle A$_1$ [8]
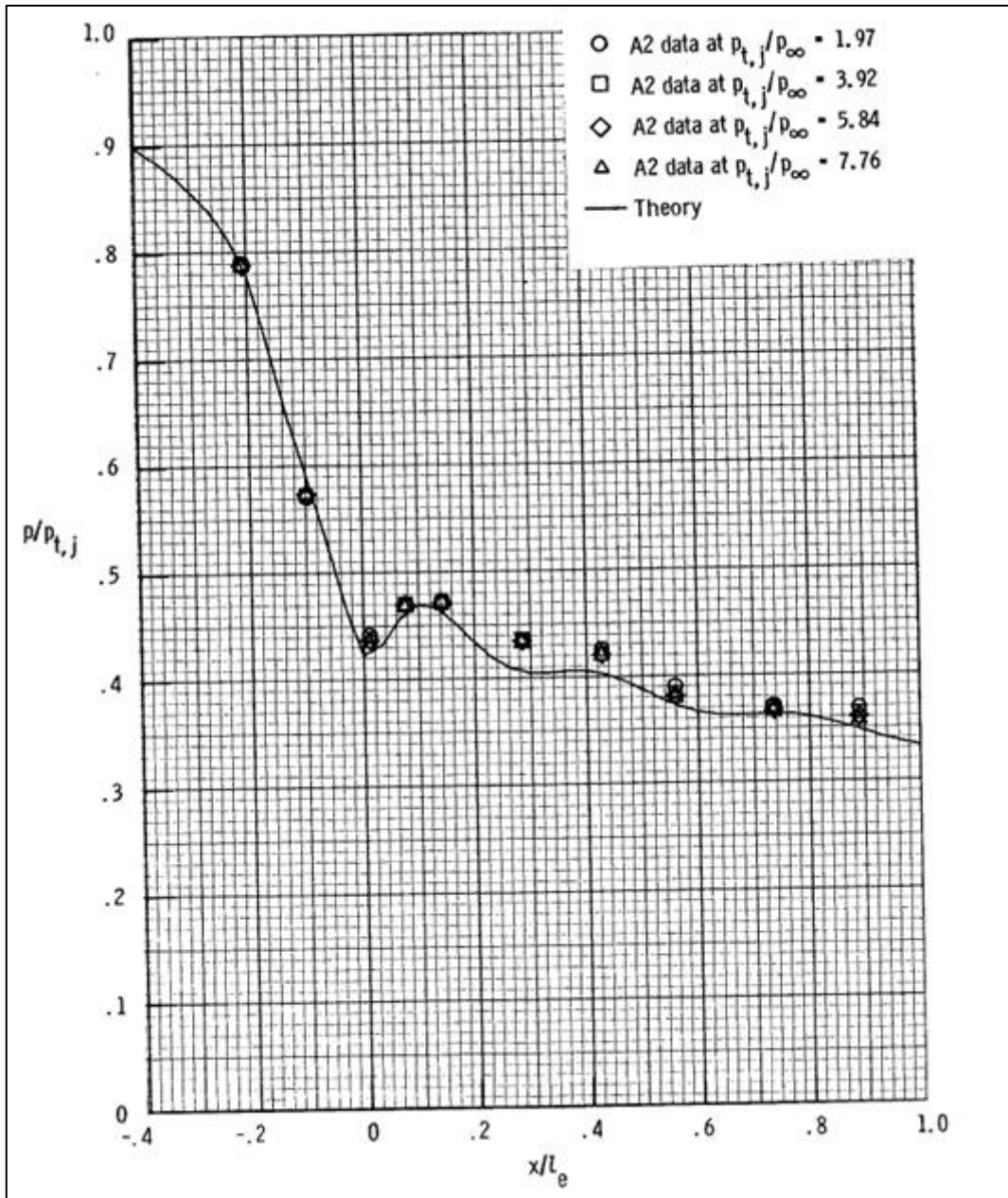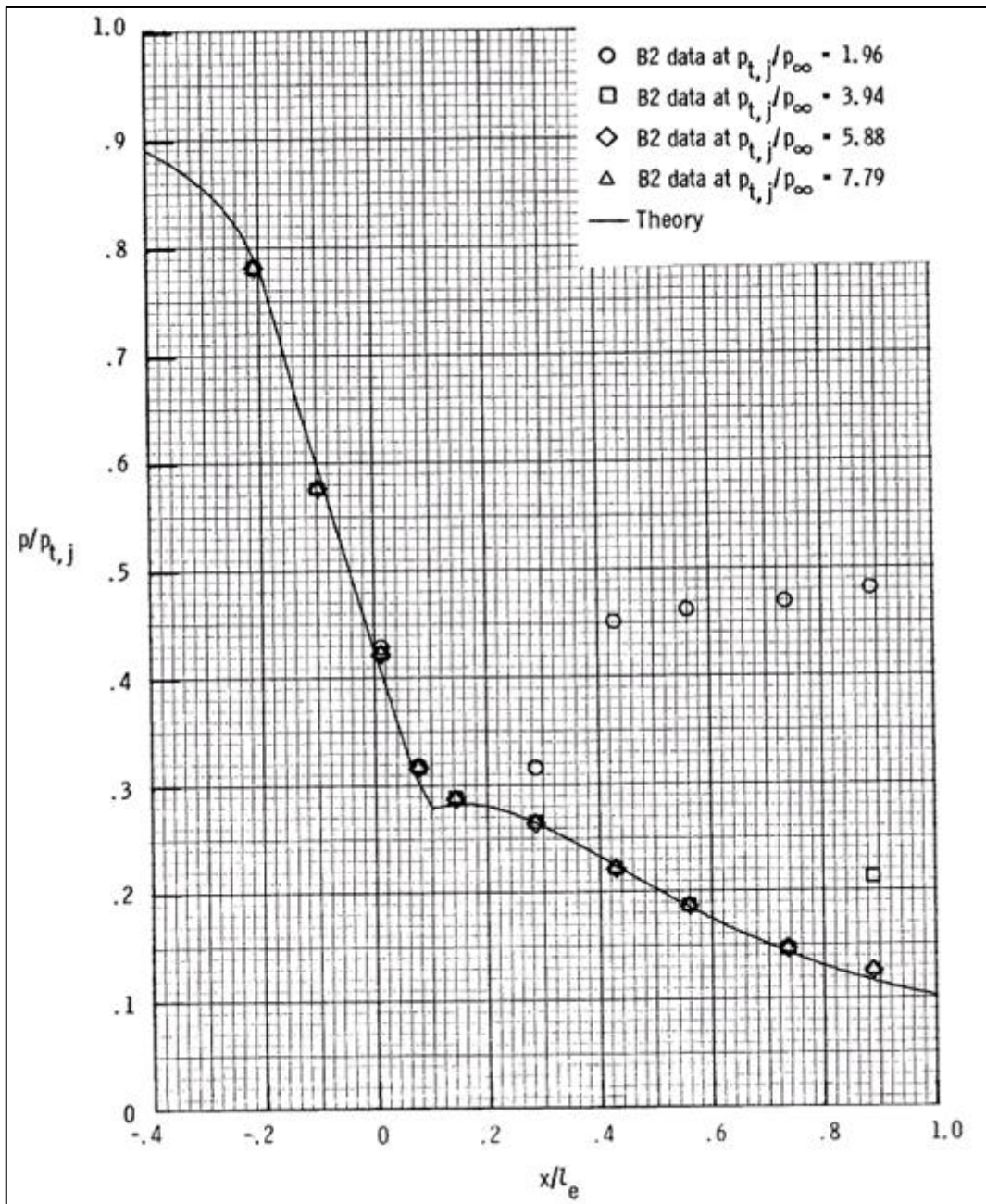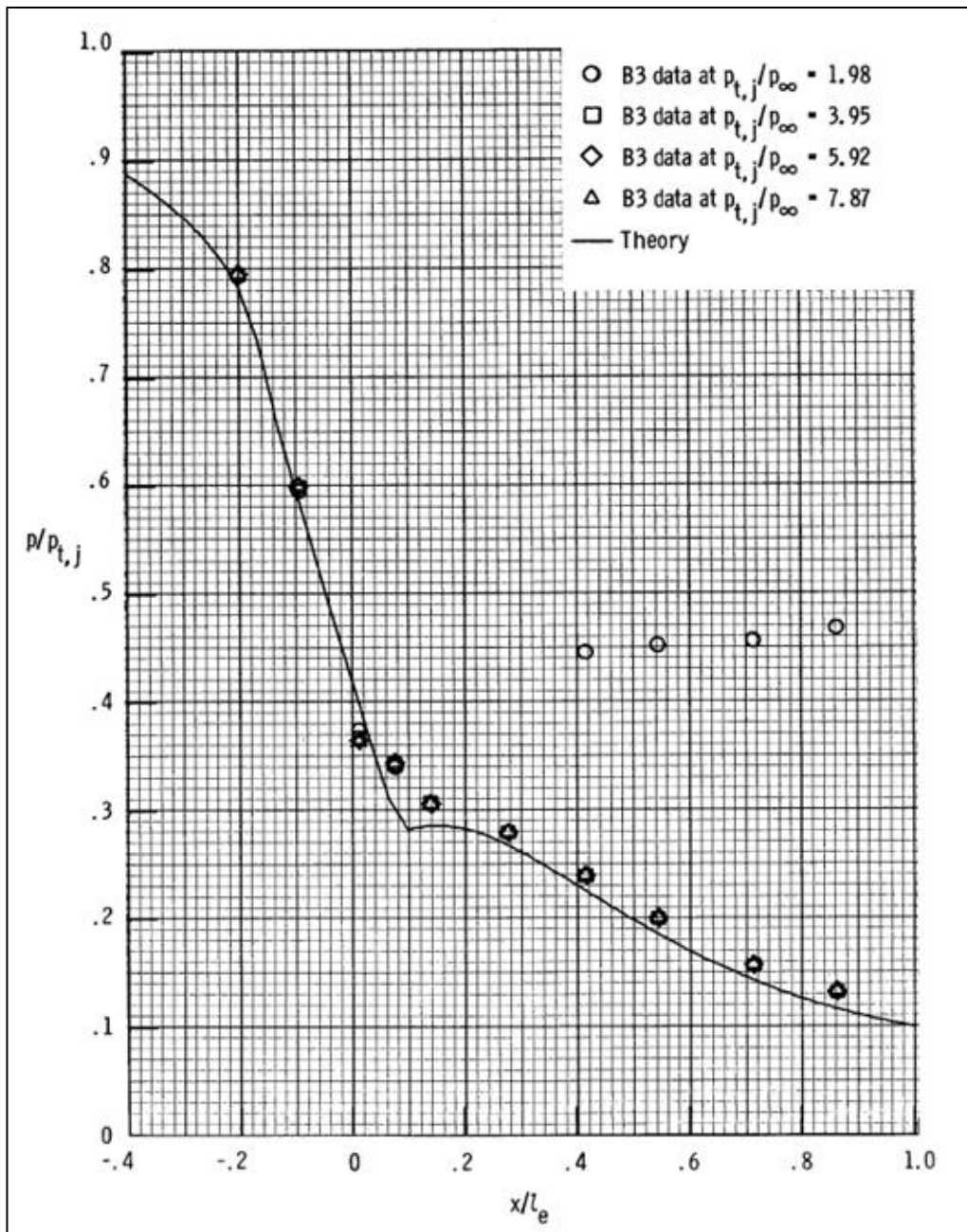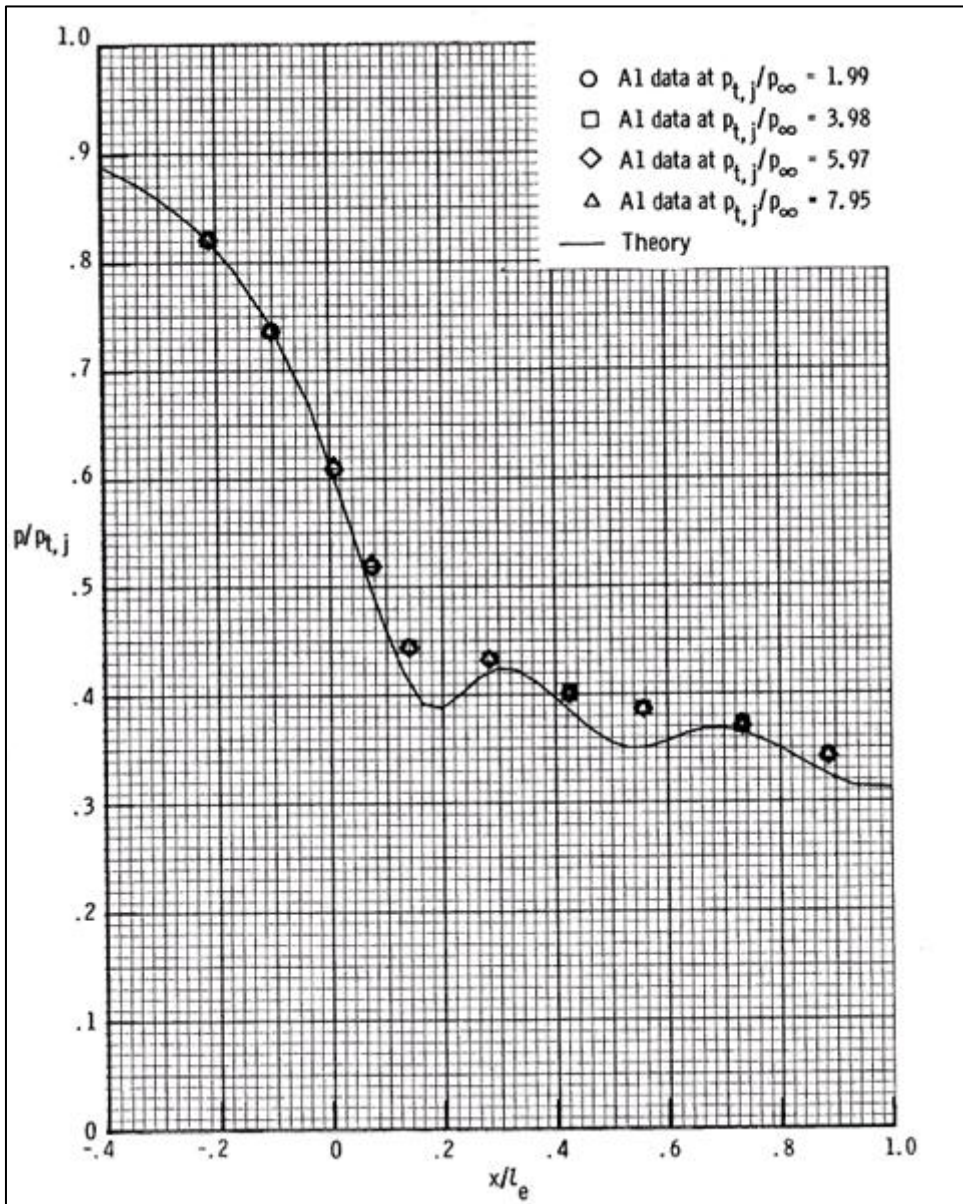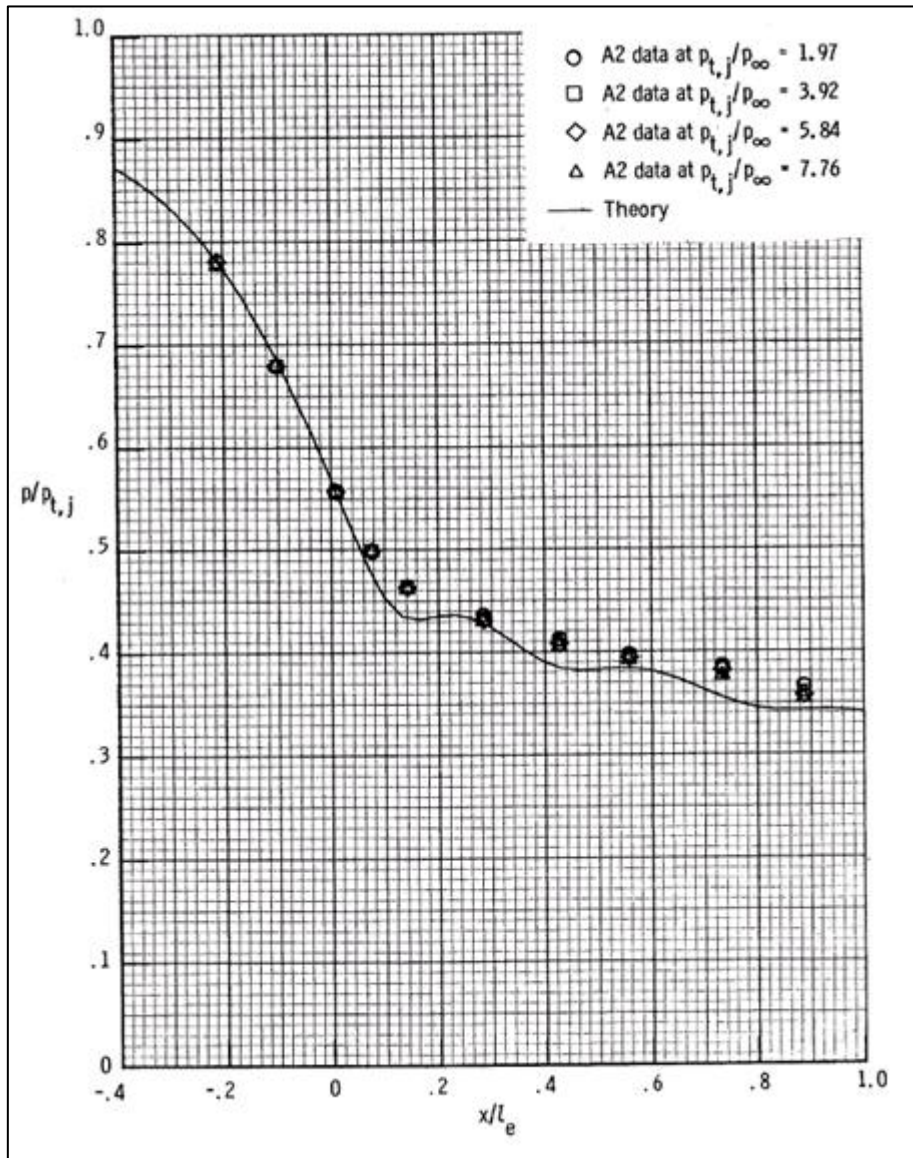
Figure A.2 Comparison of Theoretical and Experimental Static-Pressure Distributions on Center Line for Nozzle A$_2$ [8]
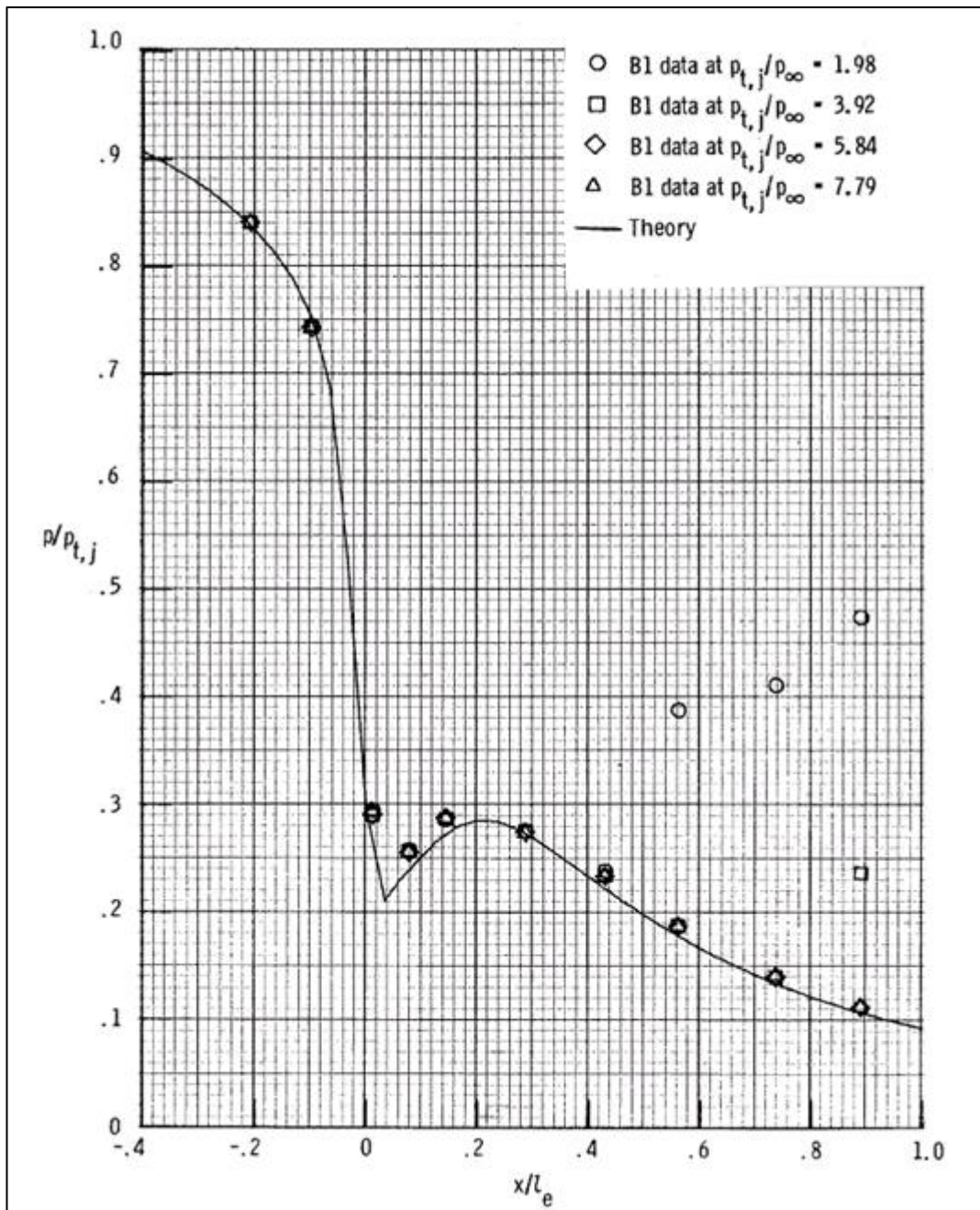
Figure A.3 Comparison of Theoretical and Experimental Static-Pressure Distributions on Center Line for Nozzle B_1 [8]

Figure A. 4 Comparison of Theoretical and Experimental Static-Pressure Distributions on Center Line for Nozzle B$_2$ [8]

Figure A.5 Comparison of Theoretical and Experimental Static-Pressure Distributions on Center Line for Nozzle B₃ [8]
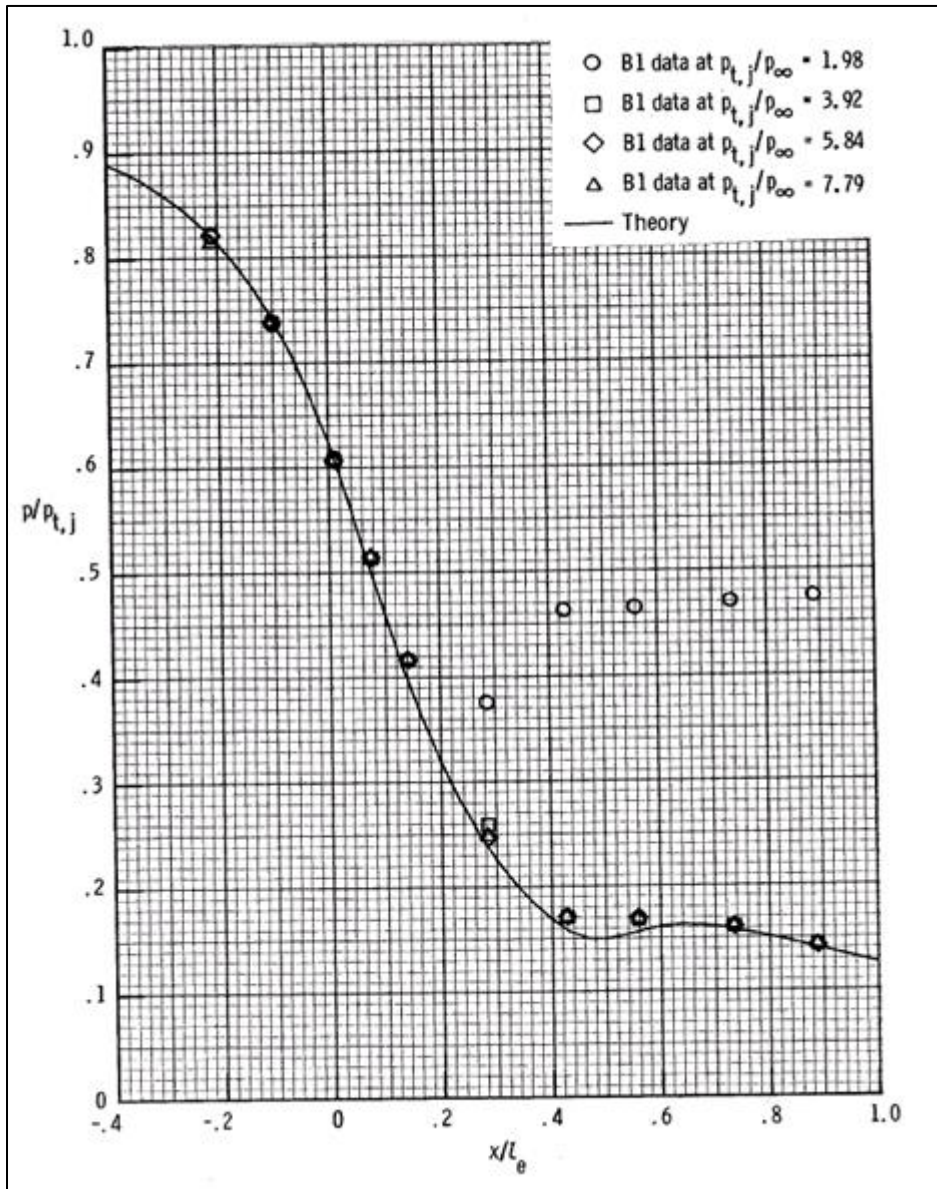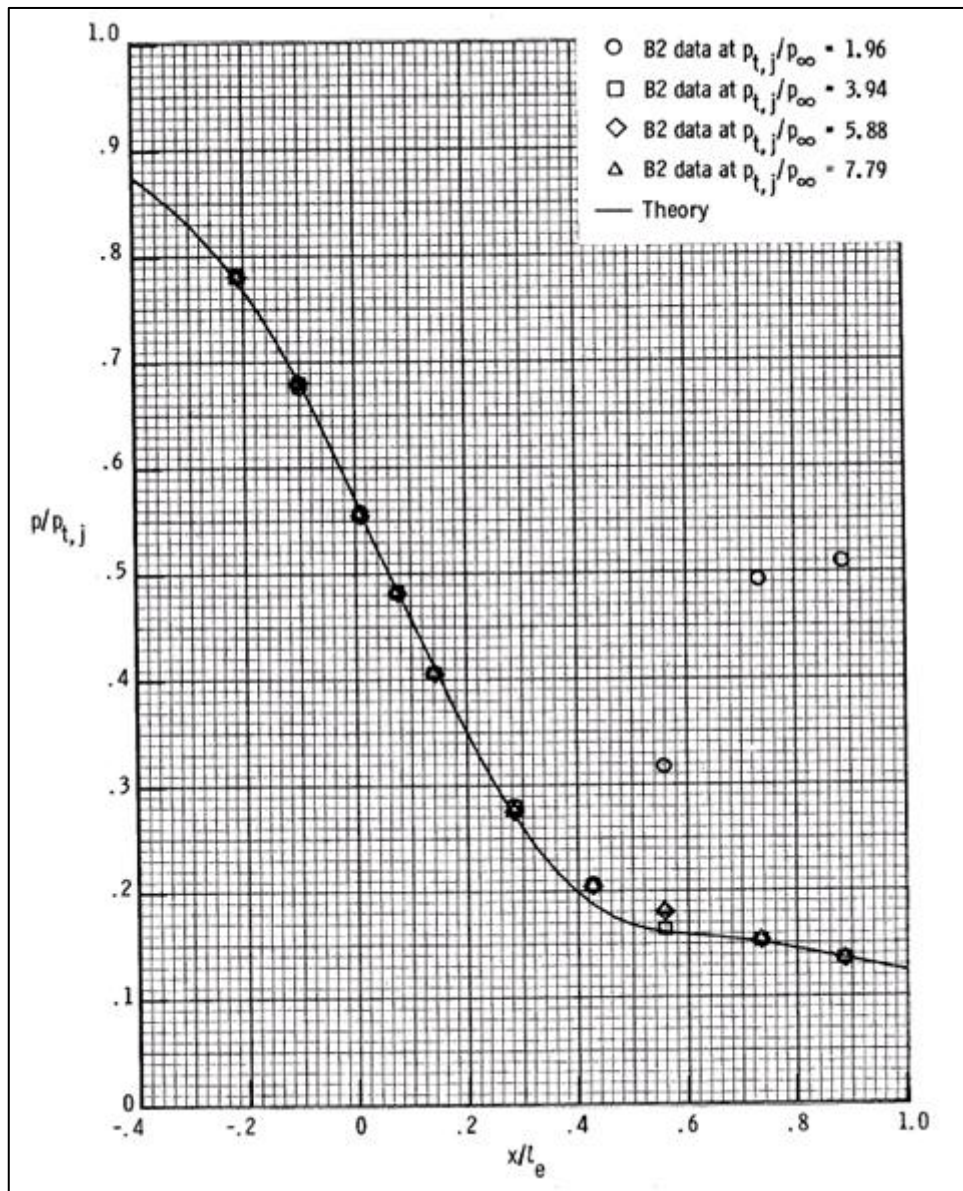
Figure A.6 Comparison of Theoretical Center Line Static Pressure Distributions with Experimental Static Pressure on Left Side Wall for Nozzle A₁ [8]
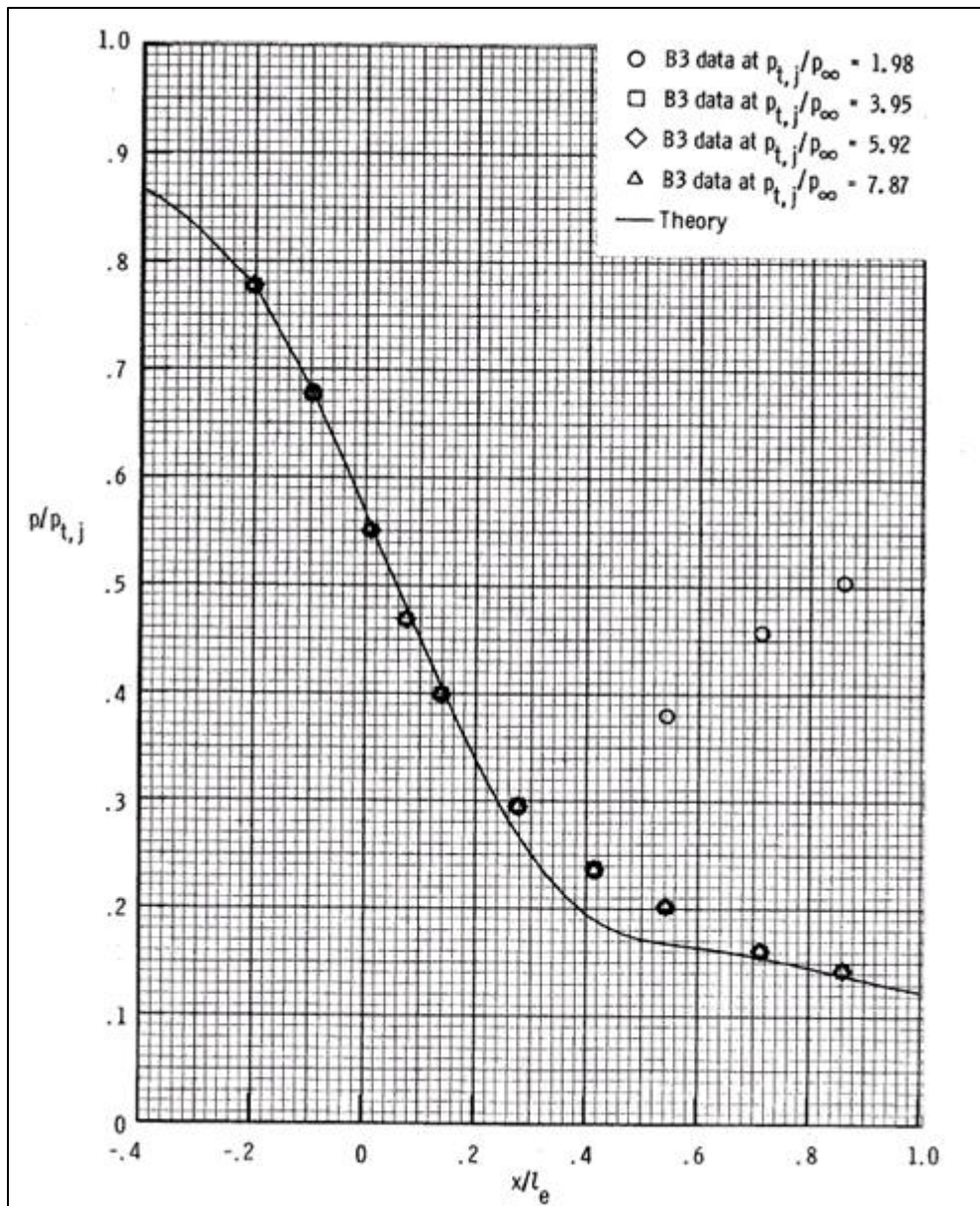
Figure A. 7 Comparison of Theoretical Center Line Static Pressure Distributions with Experimental Static Pressure on Left Side Wall for Nozzle A$_2$ [8]

Figure A. 8 Comparison of Theoretical Center Line Static Pressure Distributions with Experimental Static Pressure on Left Side Wall for Nozzle B$_1$ [8]

Figure A.9 Comparison of Theoretical Center Line Static Pressure Distributions with Experimental Static Pressure on Left Side Wall for Nozzle B₂ [8]

**Figure A.10 Comparison of Theoretical Center Line Static Pressure
Distributions with Experimental Static Pressure on Left Side Wall for
Nozzle B$_3$ [8]**

60